SYNTHESIS AND CHARACTERIZATION OF UNDOPED AND IRON DOPED BARIUM BISMITH TITANATE BY SOL-GEL PROCESS

A thesis submitted in the partial fulfillment of the requirements for the award of
Degree of Master of Engineering
in Metallurgical Engineering

Submitted By

MD FAIZAN KHAN

Examination Roll no- M4MET23001

Registration No: 160305 of 2021-2022

Under the Guidance of

Dr. SATHI BANERJEE

DEPARTMENT OF METALLURGICAL AND MATERIAL ENGINEERING
FACULTY OF ENGINEERING AND TECHNOLOGYJADAVPUR UNIVERSITY
KOLKATA-700032

&

Dr. SOUMYA MUKHERJEE

DEPARTMENT OF METALLURGICAL ENGINEERING
SCHOOL OF MINES AND METALLURGY
KAZI NAZRUL UNIVERSITY
ASANSOL-713340

Declaration of originality and Compliance of Academic Ethics

I hereby declare that this thesis "**SYNTHESIS AND CHARACTERIZATION OF UNDOPED AND IRON DOPED BARIUM BISMITH TITANATE BY SOL-GEL PROCESS**" contains literature survey and original research work by the undersigned candidate, as a part of my M.E degree in Metallurgical and Material Engineering during academic session 2021-2023. All information in this document has been obtained and presented inaccordance with academic rules and ethical conduct. I also declare that, as required by this rules and conduct, I have fully cited and referred all material and results that are not original to this work.

Name: Md Faizan Khan

Examination Roll Number: M4MET23001

Registration No- 160305 of 2021-2022

Place-Kolkata

Date- 12/06/2023

Signature-

CERTIFICATE

This is to certify that the thesis entitled "**SYNTHESIS AND CHARACTERIZATION OF UNDOPED AND IRON DOPED BARIUM BISMITH TITANATE BY SOL-GEL PROCESS"** has been carried out by Mr. Md Faizan Khan (Examination Roll: M4MET23001 and Registration No. 160305 of 2021-2022) under my guidance and supervision and accepted in partial fulfilment for the degree of Master of Engineering in Metallurgical Engineering from Jadavpur University. To the best of our knowledge the contents of this thesis or any part thereof have not been previously submitted for the award of any degree or diploma.

---------- **Prof. Pravash Chandra Chakraborti**
Head of the Department, Department of Metallurgical and Material Engineering, Jadavpur University, Kolkata-700032

---------- **Dr. Sathi Banerjee**
Associate Professor Department of Metallurgical and Material Engineering, Jadavpur University, Kolkata- 700032

---------- **Dr. Soumya Mukherjee**
Assistant Professor Department of Metallurgical Engineering, Kazi Nazrul University, Asansol- 713340

---------- **Prof. Ardhendu Ghoshal**
Dean Faculty of Engineering and Technology, Jadavpur University, Kolkata-700032

Certificate of Approval

The foregoing thesis is hereby approved as a creditable study of an engineering subject and presented in a manner satisfactory to warrant acceptance as pre-requisite to the degree for which it has been submitted. It is understood that by this approval the undersigned do not necessarily endorse or approve any statement made, opinion expressed or conclusion drawn there in but approve the thesis only for which it is submitted.

Committee on final examination for the evaluation of the thesis

---

Signature of Examiners

Acknowledgement

I would like to take this opportunity to express my heartfelt gratitude to the people who supported me throughout this research project. I would like to express my sincere gratitude to my supervisor Dr. Sathi Banerjee, Associate Professor, Department of Metallurgical and Material Engineering, Jadavpur University for her continuous support of my Metallurgical Engineering study and research, for her patience, motivation and immense knowledge. Her guidance helped me in all the time of research and writing of this thesis.

I'm deeply indebted to Prof. Pravash Chandra Chakraborti, Head of Department of Metallurgical & Material Engineering whose help, stimulating aspiration helped me throughout the period of my project work.

I also deeply acknowledge the help and guidance from Dr Soumya Mukherjee, Assistant Professor, Department of Metallurgy, Kazi Nazrul University, Asansol and Partha Sarathi Das throughout the length of my M.E project and convey my heartfelt gratitude for his guidance and support with his immense knowledge of the subject.

I also pay my indebt acknowledgement to my parents for providing needless support and aspiration during my thesis work. Finally, I take this occasion to thank all my classmates whose cooperative attitude helped me very much. I also like to acknowledge the cooperation of all the staff members of department during my project work.

Name- Md Faizan Khan

Place- Kolkata

Abstract

Sol-Gel route using AR Grade precursors are used to synthesize Barium Bismuth Titanate ceramics. The intermediate gel obtained is made to undergo thermal analyses by DSC- TGA to yield information on crystallization of ceramic phase development. Heat treatment of gel is carried in air atmosphere at about 600°C, 550°C, 500°C for 4 hours, 6 hours and 5 hours respectively. Phase developed by heat treatment is confirmed from XRD as per JCPDS standard file. Crystallite size is estimated by Scherrer's formula while planes are indexed as per feasibility of thermodynamic stability. Optimized condition for high purity indexed phase development is obtained at about 500°C for 5 hours duration. Bonding analysis is carried by FTIR analyses to determine M-O co-ordinations. Both XRD and FTIR analysis corresponds with the experimental findings to elucidate the ceramic formation. PL Test is done to get absorbance and emission spectra of BBiT, a band gap of 1.78 eV is observed with excitation and emission being 350 nm and 696 nm. FESEM analysis exhibits the morphological features of the synthesized sample and micro-structural evolution with heat treatment temperature and duration. Dense agglomerates with irregular polygonal, spherical to flaky structure are noted in some portions of the micro-structural evolution of the synthesized sample. Iron doped Barium Bismuth Titanate is synthesized using Ferric Nitrate Nonahydrate. XRD shows shifting of peaks at higher angle. Particulates are some plates like shape with some spherical condensed agglomerates.

Table of Contents

List of Figures

List of Tables

CHAPTER 1
Introduction
1.1 About BBiT and Its characteristics

$BaBi_4Ti_4O_{15}$ (BBiT), a ferroelectric compound, is a member of the known as Aurivillius family. Since this type of ferroelectrics have a layered structure with good fatigue endurance, it is possible to tail their properties and avoid many issues related to earlier ferroelectric memories [1] [2] [3] [4] [5]. Because of its distinctive crystal structure and the ensuing anisotropic electric properties, the Aurivillius family, generally denoted by the formula $Bi_2A_{m-1}B_mO_{3m+3}$, has drawn more attention. Its crystal structure has been described as a usual intergrowth of perovskite-like $(A_{m-1}B_mO_{3m+1})^{2-}$slabs and $(Bi_2O_2)^{2+}$ layers. The number of perovskite-like slabs incorporated between the $(Bi_2O_2)^{2+}$ and A in these compounds, where A is a monovalent, divalent, or trivalent element making dodecahedral coordination, B shows tetravalent, pentavalent, or hexavalent ions suitable for octahedral coordination, along with m is an integer ($1<m<5$), represents the number of perovskites [6] [7] [8] [9].

Due to their high Curie temperatures, superior polarisation fatigue resistance, and low operating voltages, the Bi-based Aurivillius family of compounds have drawn a lot of interest as materials for piezoelectric resonators, sensors, and ferroelectric random-access memory (FRAM). Currently, the most significant class of materials utilised in transducers, sensors, actuators, and so on that operate based on an electrical signal is ferroelectric (FE) solids, and these are typically polycrystalline ceramics. Subsequent photonic applications will require the identical functional performance as well as light transparency in the materials [10] [11] [12] [13]. Barium Bismuth Titanate is being developed at lower temperatures to meet this need. This class combines the well- known easy formability, optical transparency, and low cost of glasses with several nonlinear and cross-effects (such as electro-optic, second harmonic generation, etc.) exhibited by ferroelectric single crystals. Among the various methods adoptedto synthesis of ferroelectric materials, the sol-gel route has attracted considerable attention in recent decades. Fabrication of ferroelectric Barium Bismuth Titanate, using melt quenching followed by heat treatment is a popular technique to obtain pore-free, fine-grained, nano/micro- structured material embedded in a low permittivity, high resistivity host glass matrix. With this method, strict control over the crystallite size is possible and transparent characteristics of BBiT can be retained [14].

There are a number of advantages in preparing these materials through this technique which includes the use of a low-cost and high-speed fabrication process,the absence of pores that impart these materials, higher mechanical and dielectric breakdown strengths and the possibility of altering the properties by varying the volume fraction of the active phase dispersed in the glass matrix and its micro/nano structures. On the other hand, the volume fraction of the ferroelectric phase and the grain size, which are critical parameters in dictating the properties of the materials, can be controlled by the composition and heat treatment process.

In order to improve performance and protect the environment, there is a lot of interest in changing the current generation of thin film ferroelectrics, which are based on perovskites like lead zirconia titanates (PZT). When compared to PZT, the Aurivillius oxides, like BBiT, exhibit better fatigue-free behaviour and have lower coercive fields because they don't contain the hazardous heavy metal lead. BBiT ceramics are synthesized mainly by chemical, mechanochemical and solid-state reactions.

The objective of the present investigation is synthesis of Barium Bismuth Titanate ($BaBi_4Ti_4O_{15}$) by Sol-gel process and evaluation of its different characteristics [15].

1.2 Sol-Gel Process

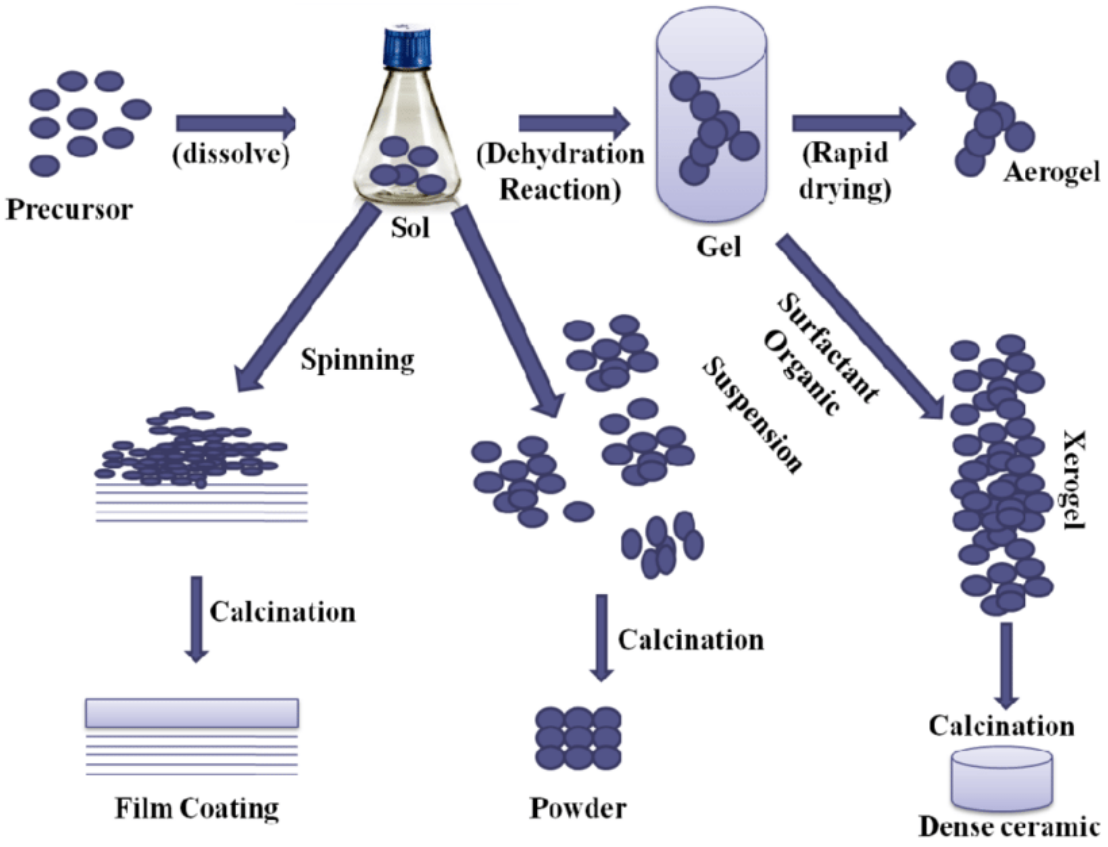

Figure 1: Sol-gel process chart

The sol-gel process may be described as formation of oxide network through hydrolysis and polycondensation reactions of a molecular precursor in a liquid. Sol is a stable dispersion of colloidal particles of polymers in a solvent. Gel consists of a three-dimensional network, which contains a liquid phase [16].

1.2.1 Advantages of Sol-Gel process

- Versatile: Better control over the structure, which includes porosity and particles size; potential to incorporate organic compounds and nanoparticles into oxides derived from sol-gel.
- Extended composition ranges: These enable the production of any oxide composition as well as some non-oxides and the creation of novel organic-inorganic hybrid materials that do not naturally exist.
- Superior homogeneity: due to blending at the atomic level; highly pure
- It is not necessary to attain the melting temperature as the desired network arrangement can be attained at temperatures that are relatively low, in proximity to the glass transition temperature (Tg), resulting in reduced consumption of energ y
- Various forms of materials including coatings, thin films, monoliths, composites, porous membranes, powders and fibers are commonly utilized in diverse areas of research and industrial applicati ons.
- There is no requirement for the use of specialized or highly priced instrumentation.

1.2.2 Disadvantages of Sol-Gel process

- Cost of precursors are high
- Shrinkage of a wet gel upon drying, which often leads to fracture due to the generation of large capillary stresses and, consequently, makes difficult the attainment of large monolithic pieces
- Preferential precipitation of a particular oxide during sol formation (in multi component glasses) due to the different reactivity of the alkoxide precursors
- Difficult to avoid residual porosity and OH groups

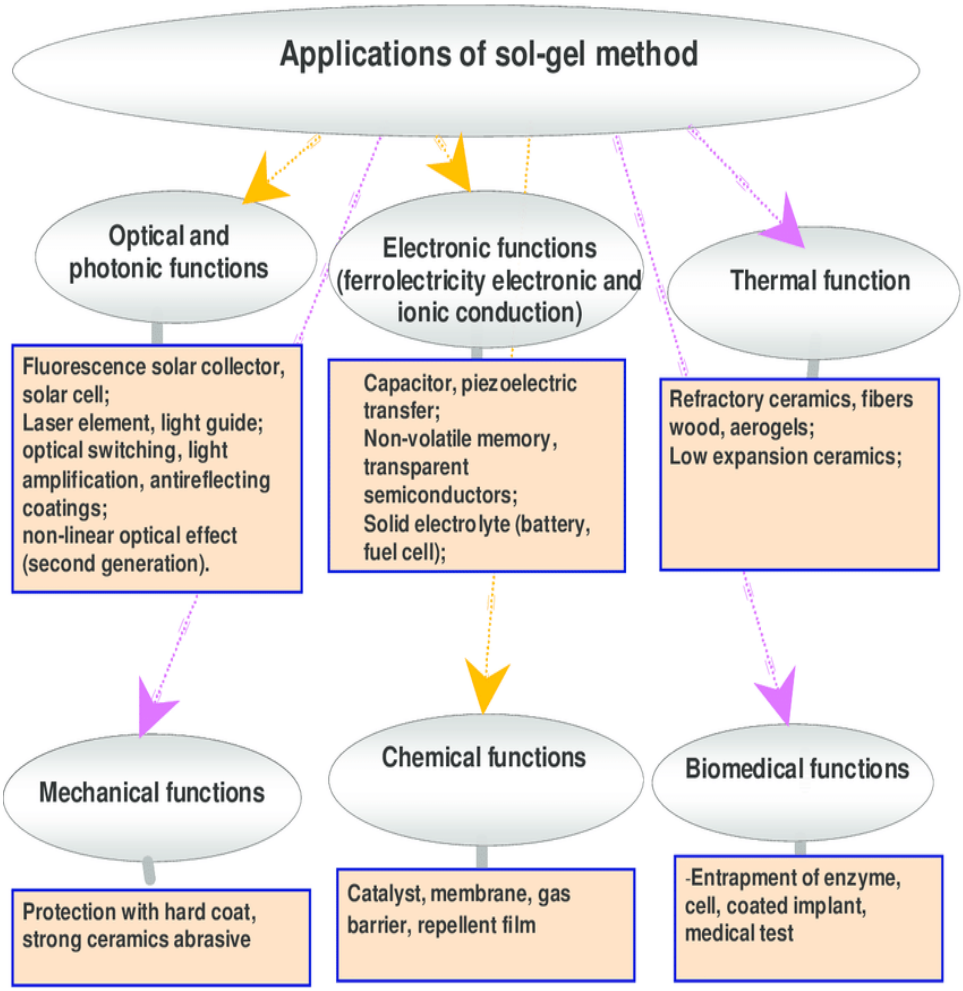

Figure 2: Application of Sol-gel process

1.3 Ferroelectric Materials

Certain materials have a unique property called ferroelectricity, where they naturally display a reversible electric polarization when exposed to an external electric field. All ferroelectrics possess the capability of pyroelectricity, which is accentuated by their electrical polarization that can be reversed. Both the aforementioned term and ferromagnetism describe materials that exhibit an uninterrupted magnetic moment in comparable ways. The phenomenon of ferromagnetism was already in existence by the year 1920 when Joseph Valasek made the discovery of ferroelectricity in Rochelle salt. Therefore, it was common practice in the field to utilize the prefix "ferro," denoting pertaining to iron, to characterize the property of ferroelectricity, despite the reality that the majority of ferroelectric substances lack any presence of iron. Multiferroics refer to materials possessing both ferroelectric and ferromagnetic properties [17] [18].

Ferroelectric Materials and Their Properties

- Dielectric Constant/Permittivity
- Dielectric Strength
- Remnant Polarization
- Coercive Field
- Compliance
- Piezoelectric Charge Constant or Piezoelectric Coefficient
- Piezoelectric Voltage Constant
- Electromechanical Coupling Factor

Ferroelectric materials exhibit numerous intriguing characteristics that are contingent upon a variety of factors, including electric field intensity, temperature changes, mechanical strain, and additional parameters. Hence, they exhibit considerable utility in a diverse range of applications, encompassing capacitors, memory cells, sensors, actuators, energy storage, and beyond.

Applications of Ferroelectrics

- Non-Volatile RAMs (memory)
- Dynamic RAMs (capacitors)
- Tunable Microwaves Devices
- Pyroelectric Detectors/Sensors
- Optical Waveguides
- Piezoelectric Sensors/Actuators, MEMS

1.4 Aurivillius Phases

The Aurivillius phases are a type of perovskite material explicated by the general chemical formula $(Bi_2O_2)(A_{n-1}BnO_{3n+1})$, in which A denotes a large 12-coordinate cation and B represents a small 6-coordinate cation. The fundamental arrangement consists of alternating tiers of $[Bi_2O_2]^{2+}$ and pseudo perovskite blocks, with perovskite sheets possessing a thickness equal to n octahedral layers. In 1949, the Swedish chemist Bengt Aurivillius was the initial scholar to provide a description of the crystal structure. The initial fascination with Aurivillius phases emerged from the detection of ferroelectric behavior exhibited by Bi2WO6 (n=1), the most elementary member of this crystallographic family. The Aurivillius phase Bi2MoO6, homologous to molybdenum, has been the subject of recent investigations as a viable material for application in low-temperature co-fired ceramics (LTCC). The oxide ion-conducting properties exhibited by Aurivillius phases were initially discovered by Takahashi et al. in the 1970s. Since then, they have been utilized extensively for this purpose. Aurivillius phase oxide materials constitute a subclass of ceramics that are free of lead [19].

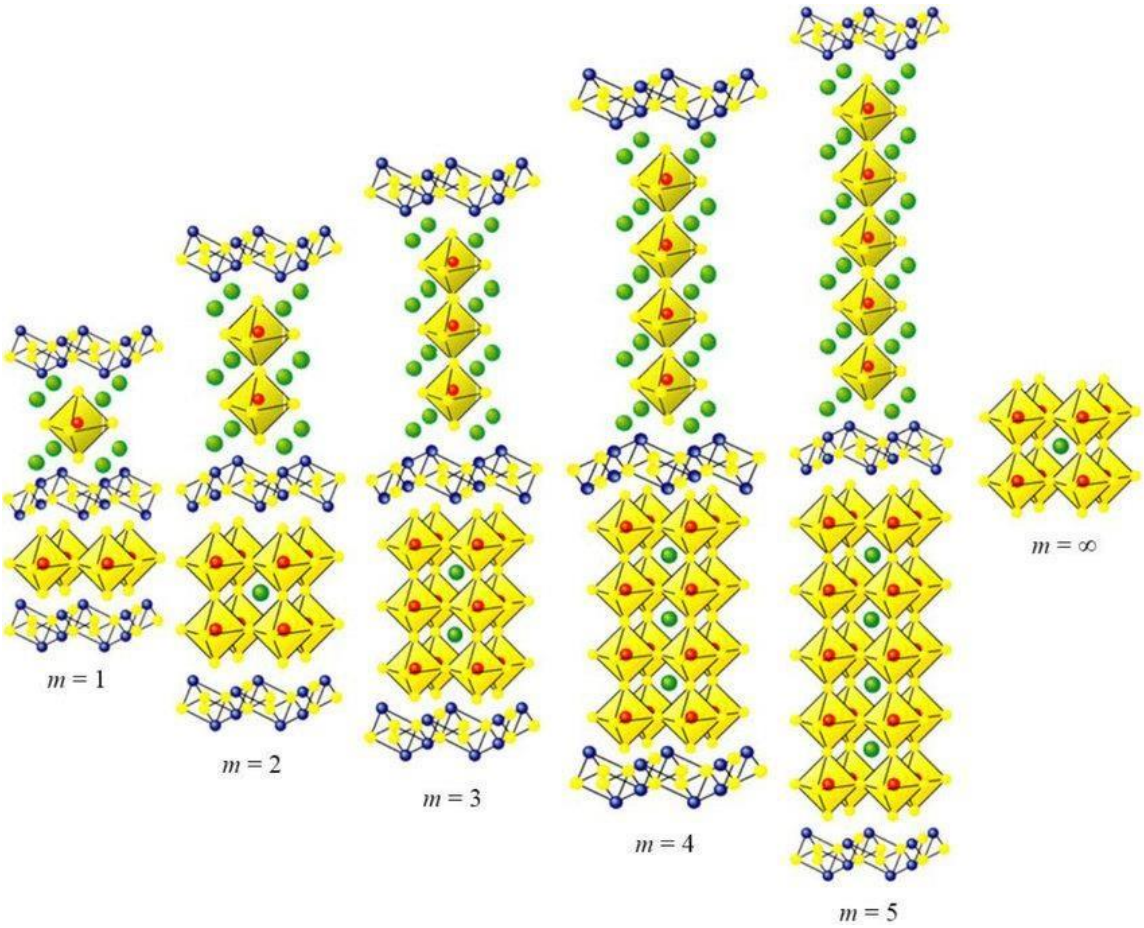

Figure 3: Aurivillius phase structure

CHAPTER 2
Literature Review

2.1 Method of synthesis of Barium Bismuth Titanate

2.1.1 Sol-Gel Method

BBiT thin films can be produced on silicon substrate using a modified Sol-Gel method. A major problem of Sol-Gel processing is the chemical reaction and mechanism of precursor solution. Ethanolamine is an effective complexation reagent of Bi^{3+}, which could control the acidity of precursor. It is found that when pH value is about 3.5, the stable and uniform BBiT precursor could be obtained. Using such precursor, smooth and uniform BBiT thin films can be obtained. The Bi-layered perovskite structure of BBiT forms at 750°C. The morphology of the grains in BBiT thin films is generally spheroidal and the grain size is about 120 nm.

Barium Bismith Titanate is made through an experiment using, Barium Acetate ($Ba(CH_3COO)_2$), Bismuth Nitrate($Bi(NO_3)_3{\cdot}5H_2O$) and Tetrabutyl Titanate ($Ti(OC_4H_9)_4$) are used as starting materials. The solvents chosen for this study were Glacial Acetic acid (CH_3COOH) and Ethanol (CH_3CH_2OH), while the complexation reagent used was Ethanolamine ($H_2NCH_2CH_2OH$) and the reagent for stabilizing Tetrabutyl Titanate was Acetylacetone ($CH_3COCH_2COCH_3$). In order to prevent the excessive hydrolysis of Ti(OC4H9)4, the 99% pure $Bi(NO_3)_3{\cdot}5H_2O$ is vacuum-dried at 60ºC for 96h. And then solved in glacial acetic acid. After the solution become transparent, they are mixed with $Ba(CH_3COO)_2$ acetum. The compound Acetylacetone is employed as a means of stabilizing Tetrabutyl Titanate. Thereafter, the stabilized Tetrabutyl Titanate is subjected to modifications and added to a mixed solution of Bi-Ba acetum. This addition is carried out with a continuous stirring process, maintaining the temperature of the mixture at room level. In order to modify the viscosity of a solution, it is necessary to decrease the surface tension of the precursor substance, as well as inhibit the hydrolysis of Bismuth Nitrate in Acetic acid. To accomplish this, Ethanolamine is introduced into the solution with the aid of ultrasonic agitation. pH value is adjusted using Glacial Acetic acid to remain about 3.5. The resultant solution is filtered to form the stock solution, which is transparent, yellow and clear [20].

In the formation process of precursor, $Bi(NO_3)_3$ is very easy to yield a white precipitate ($BiONO_3$) due to Bi^{3+} reacts easily with H_2O. Therefore, the liquid is unstable and decomposes evidently in a few hours. Through lots of experiments, it is found that the addition of Ethanolamine can adjust the pH value of the solution. The solution obtained exhibited remarkable stability with respect to precipitation, suggesting that Ethanolamine demonstrates the capacity to impede the hydrolysis of $Bi(NO_3)_3$. In acidic solution, $Bi(NO_3)_3$ reacts with $H_2NCH_2CH_2OH$ to yield Bismuth complex as follows:

$$Bi^{3+} + 4H_2NCH_2CH_2OH \rightarrow [Bi(H_2NCH_2CH_2OH)_4]^{3+}$$

Because the Bismuth complex is very stable, it prevents hydrolysis of Bi^{3+}. When pH value is about 3.5, the stable BBT thin films are obtained. When pH value is lower or higher than 3.5, $Bi_{12}TiO_{20}$ phase appears.

The present findings demonstrate that an increase in the pH value of the solution augments the rate of hydrolysis of Ti(OC4H9)4, consequently leading to the precipitation reaction as represented below.

$Ti(OC_4H_9)_4 + H_2O \rightarrow Ti(OH)_4 \downarrow + 4C_4H_9OH$

In such solution environment, it is easy for Ti^{4+} to combine with Bi^{3+}, which will lead to the formation of Bismuth Titanate mixed phases. Therefore, it is essential to control the hydrolysis of $Ti(OC_4H_9)_4$.

The stable complex, acetylacetone is selected for its favorable property of stabilizing $Ti(OC_4H_9)_4$. It is found that the evident vibration peaks appear at 1200~1720 cm^{-1} range in Ba-Bi-Ti system stabilized by Acetylacetone. Therein, the peak at 1704 cm^{-1} is due to the symmetry and asymmetry flexing vibration of hydroxyl (-COO-). And the peak at 1557 cm^{-1} is formed by the coupling interaction of Ti^{4+} and Acetylacetone.

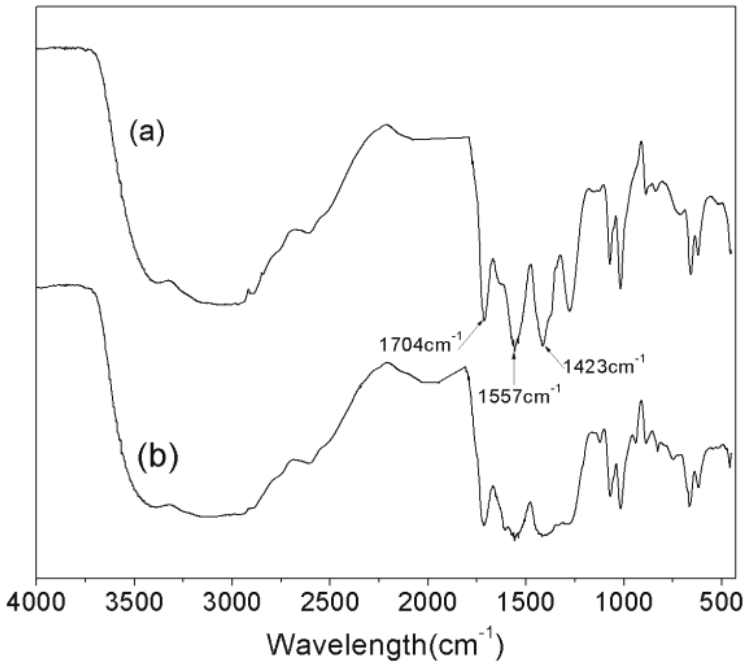

Figure 4: IR spectra of precursor solution before and after adding Acetylacetone

Also, when Ti^{4+} reacts with Acetylacetone, the stable coupling structure will be formed by overlapping effect of hydroxyl bond. Below fig 6 shows the structure of Acetylacetone titanium [21] [22].

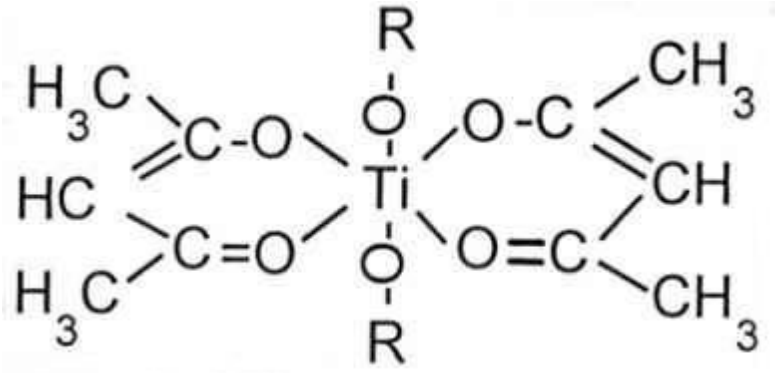

Figure 5: Structure of Acetylacetone titanium

2.1.2 Mechanochemical Synthesis

The intrinsic characteristic of this technique is that the solid-state reaction is activated via mechanical energy instead of heat energy (high temperature). There exist various benefits of the mechanical synthesis process. Firstly, this method utilizes economical and readily accessible oxides as the raw materials and obviates the need for an intermediate temperature calcinations phase, therefore simplifying the process [12]. Secondly, it takes place at a temperature close to room temperature in a sealed container. Moreover, the powders obtained through mechanical means exhibit an enhanced capability of sintering as compared to those powders produced through traditional solid-state reactions and a substantial majority of wet-chemical techniques.

The implementation of mechanical activation proves to be an efficacious technique for acquiring nanostructure powders, particularly with respect to the pursuit of miniaturization and integration of electronic components. The conventional method of ceramic synthesis can result in non-stoichiometric composition of the BIT powder due to the undesirable loss of bismuth content via Bi_2O_3 volatilization that occurs at high temperatures [23] [24].

BBiT is prepared from stoichiometric quantities of BT and BIT obtained via mechanochemical synthesis. BT is synthesized from mixture of BaO and TiO_2 in anatase crystal form and BIT was prepared starting from Bi_2O_3 and TiO_2, the same type such as for BT [24]. Mechanochemical synthesis is performed in air atmosphere in a planetary ball mill. BT powder was created after one hour of milling, and BIT powder after six hours. The operating parameters for milling are as follows: utilization of zirconium oxide jars and zirconium oxide balls, with a ball-to-powder weight ratio maintained at 20:1. The basic disc rotation speed is set at 320 min^{-1}, while the rotation speed of discs with jars remains fixed at 400 rpm. The balls utilized in milling have a diameter of 10 mm. The powder mixture of BT and BIT is homogenized for 30 min (speed 142 min^{-1}) and then pressed into pellets using a cold isostatic press (8 mm in diameter and 3 mm thick). Their powder mixture is sintered at 1100°C for 4 h without the pre-calcinations step. The heating rate is 10°C min^{-1}, with natural cooling in air atmosphere. Separately, BIT is sintered at 1000 °C for 12 h and BT is sintered at 1300 °C for 2 h.

Bi-layered structure ferroelectric material-bismuth titanate, $Bi_4Ti_3O_{12}$ (BIT) and barium-bismuth titanate, $BaBi_4Ti_4O_{15}$ (BBiT) ceramic powders is prepared by the mechanical synthesis process. XRD shows that synthesized BBiT has a tetragonal structure of an Aurivillius phase Bi-layered oxide. Only 4 Raman bonds were clearly observed. It is evident that Ba^{2+} addition leads to the change in microstructure development. $BaBi_4Ti_4O_{15}$ with good crystalline structure was formed after sintering without a pre-calcination step with a plate-like structure typical for layered structure materials [25].

2.1.3 Modified Solid State Route

The primary methods used in the synthesis of BBiT ceramics are chemical and solid-state reactions techniques. The polymeric precursors-Pechini process, sol-gel, co-precipitation, and hydrothermal method-are the most frequently used chemical techniques. BBiT can be also produced by conventional solid-state reaction starting from $BaCO_3$, TiO_2, Bi_2O_3 [26] [25] [10] [2]. For the preparation of ceramic powder, the solid-state reactions started by vigorous milling in high-energies ball mills might be a good option. A critical criterion for intense milling is the production of dispersed phased substances, which is characteristic of metal powders or materials composed of oxides,

through mechanical activation. Alternatively, mechanochemical synthesis can lead to the creation of other products via solid-state reaction. The process of intensive milling facilitates a significant augmentation in the contact area among reactant powder particles by virtue of the marked decrease in particle dimensions. This in turn enables the exposure of fresh surfaces, thereby enabling more extensive contact between particles. The aforementioned phenomenon facilitates the process of reduction to occur without the prerequisite of diffusion through the layer of the resultant product. [25] Mechanochemical synthesis has been observed to facilitate solid-state reactions at comparatively lower temperatures, without any need for external heating. This phenomenon represents a significant deviation from the conventional expectation of elevated temperature requirements for such reactions.

The precursor materials required for synthesis are AR grade Barium oxide, Bismuth Oxide and Titania. The experiment commenced by combining the precursors in appropriate molar proportions of $BaO:Bi_2O_3:TiO_2$ in a ratio of 1:2:4, followed by subjecting the resultant mixture to extensive milling in an agate mortar for mechanochemical activation. Milling is generally carried for 20 hours, 25 hours and 30 hours respectively. After milling powder samples are put into tubular furnace in presence of air atmosphere for annealing. The annealing process was conducted at a temperature of 700°C, with varying soaking durations of 10 hours, 8 hours, and 6 hours, respectively. Prior to annealing, the powder samples underwent different milling durations of 20 hours, 25 hours, and 30 hours, respectively.
It is noted that crystallite size decreases with increase in milling time while the soaking period decreases at constant annealing temperature.

2.2 Influence of Doping on Barium Bismuth Titanate

2.2.1 Lanthanum Doping

Polycrystalline Barium Lanthanum Bismuth Titanate (BLBT), $Ba_{1-(3/2)x}La_xBi_4Ti_4O_{15}$, powders of various compositions x = 0, 0.05, 0.1, 0.2, 0.3 and 0.4 can be synthesized via the conventional-solid state reaction route.

The monophasic nature of the aforementioned compositions and their association with the m = 4 Aurivillius family of oxides were validated via X-ray powder diffraction analysis. The effect of the partial presence of La^{3+} on Ba^{2+} sites on the microstructure, dielectric and relaxor behaviour of $BaBi_4Ti_4O_{15}$ (BBiT) ceramics is as follows-for the compositions pertaining to $x \leq 0.1$, the dielectric constant at both room temperature and in the vicinity of the temperature of the dielectric maximum (T_m) of the parent phase (BBiT) increased significantly with an increase in x while T_m remained almost constant. T_m shifted towards lower temperatures accompanied by a decrease in the magnitude of the dielectric maximum ($\mathcal{E}_m$) with an increase in the lanthanum content ($0.1 < x \leq 0.4$). The present study observed a considerable decrease in frequency dispersion of Tm, as a consequence of an increase in lanthanum doping. For compositions with x values equal to or exceeding 0. 3, Tm exhibited frequency independence [27].

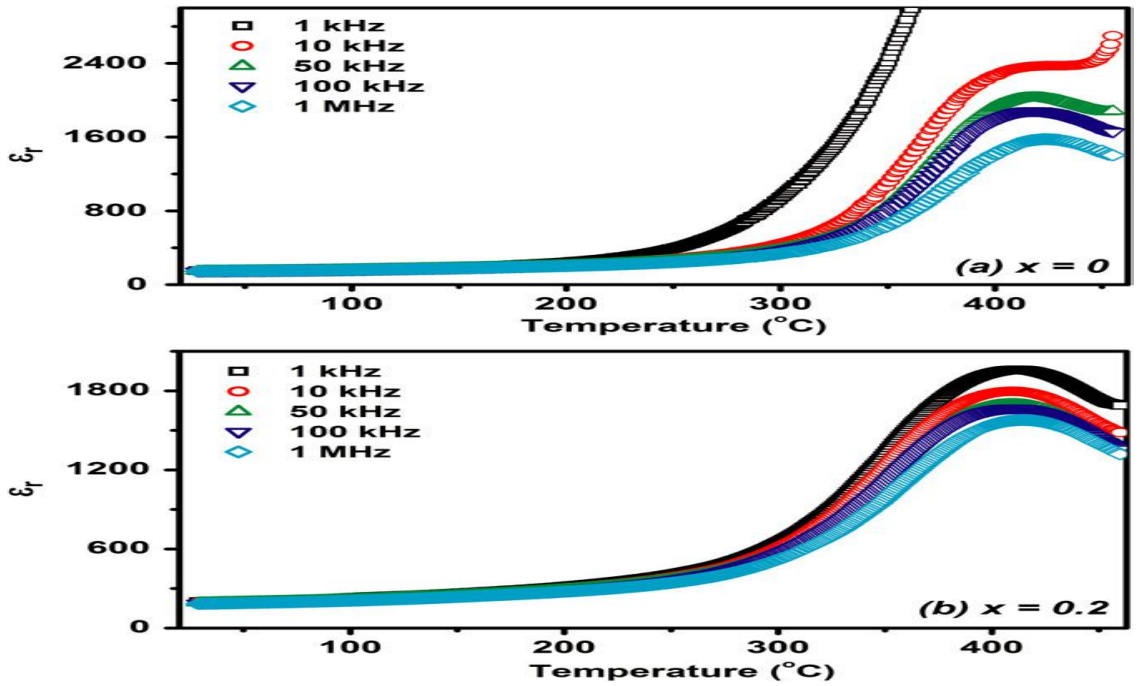

Figure 6: Temperature dependence of the dielectric constant at different frequencies for (a) x=0 and (b) x=0.2

In relaxor ferroelectrics the frequency dependence of the temperature of the dielectric peak is found to obey the Vogel–Fulcher law [28],

$$f = f_o * \exp[-E_a/k(T_m - T_{VF})]$$

where E_a and f_o are the activation energy and the attempt frequency of the dipole reorientation, respectively, and T_{VF} is the freezing temperature of the polarization fluctuations.

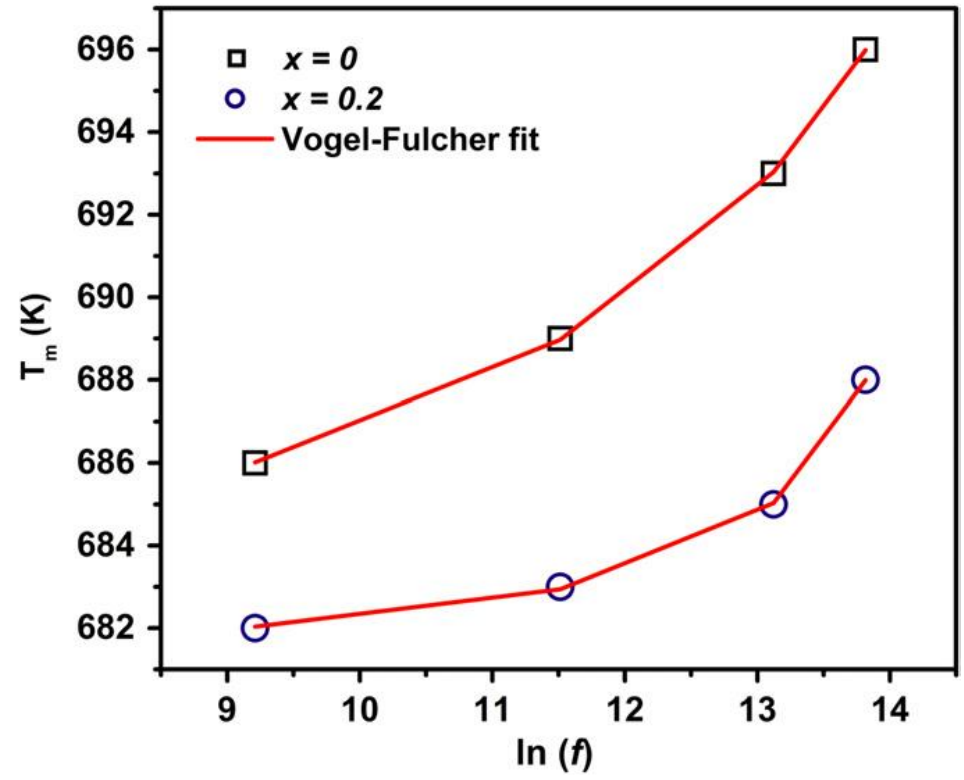

Figure 7: Temperature of the dielectric maximum Tm as a function of ln(f) for the representative compositions x = 0 and x = 0.2

Figure 7 shows the variation of the temperature of the dielectric maximum T_m as a function of ln*(f)* for the representative compositions $x = 0$ and $x = 0.2$, where open symbols represent the experimental data and the solid line is the fit to above equation. The temperature of the dielectric peak T_m shows a good fit to the Vogel–Fulcher law, showing typical relaxor behaviour.

La^{3+} doping (up to 40 mol%) do not affect the crystal structure of BBiT. However, the microstructural features such as the grain size are suppressed in the doped samples. The temperature of the dielectric maximum remained unchanged for lower concentrations of lanthanum ($x < 0.1$) and then decreased with the increase in the La content. The dielectric loss decreased with La doping, especially at higher temperatures. The diffuseness increased with increasing x and the compositions corresponding to $x = 0.3$ and 0.4 showed non-relaxor DPT. The incorporation of La^{3+} resulted in a significant reduction in dc conductivity throughout the temperature range. The increased activation energies and lower values of dc conductivities confirmed the decreased oxygen vacancy concentration [27].

2.2.2 Niobium doped Barium Bismuth Titanate

$BaBi_4Ti_{4-5/4x}Nb_xO_{15}$ (BBNTx, x = 0, 0.05, 0.15, 0.30) ceramics can be prepared by solid state method. The X-ray diffraction (XRD) results signify the establishment of homogeneous, single-layered perovskite compounds across all compositions.

Sample	ρ(1110°C)	ρ(1120°C)	ρ(1130°C)
BBiT	-	79.3%	88.9%
BBiNT 5	69.8%	80%	91.7%
BBiNT 15	72.3%	84.4%	94.9%
BBiNT 30	81.5%	95.4%	Melting

Table 1: Influence of sintering temperature on density of ceramics

The density of the samples increases with Nb doping. In the case of BBNT30 lower sintering temperature (1120°C) is needed to achieve satisfactory density (95.4%).

The effect of niobium doping on the dielectric and relaxor behaviour of $BaBi_4Ti_4O_{15}$ ceramics can be seen in a wide range of temperatures (20–777°C) and frequencies (1.21 kHz to 1 MHz) [29] [30]. The incorporation of Nb as a dopant exerts a significant influence on the Curie temperature, as well as on the reduction of the dielectric permittivity observed at the Curie temperature [31]. Undoped $BaBi_4Ti_4O_{15}$ demonstrates a dielectric constant of approximately 204 at a frequency of 100 kHz when maintained at room temperature. This value demonstrates a slight increase with the inclusion of Nb doping. The conductivity of BBNT5 ceramics is lower than that of other compositions. The value of activation energy of σ_{DC} is 0.89 eV, 1.01 eV, 0.93 eV and 0.71 eV for BBT, BBNT5, BBNT15 and BBNT30, respectively [32].

Nb^{5+} doping (up to 30 mol%) did not affect the crystal structure of BBiT. Based on the

scanning electron microscopy (SEM) micrographs, the phenomenon of grain growth was found to be inhibited in samples doped with niobium (Nb). A noteworthy enhancement in the density of the Nb-doped specimens has been observed. The ferroelectric phase transition temperature decreases with Nb contents increase, and the dielectric peak broadens (increase the parameter d from 59.6 to 115.3) showing the increase of the degree of diffuseness of the dielectric peak.

Because conducting species in every specimen are thermally activated, conductivity rises as temperature rises. The conductivity decreases for the BBNT5 to a minimum value where the concentration of electron holes matches the electron concentration (p = n). With a further increase in the donor concentration the conductivity becomes n-type and starts to increase. From impedance data one semi-circular arc, corresponding to the electrical response of grains is observed for undoped and doped sample. The broader complex plots observed in doped samples are attributed to the random arrangement of cations in the structure, leading to microscopic heterogeneity in the composition.

2.2.3 Nd^{3+} doped Barium Bismuth Titanate

Glass with a molar composition of $50KS_2.50BBiT$ (where KS_2 is $K_2O.2SiO_2$), and BBiT corresponds to $BaO.2Bi_2O_3.4TiO_2$ [$BaBi_4Ti_4O_{15}$] can be prepared from high-purity chemicals, namely SiO_2, anhydrous potassium carbonate, K_2CO_3, titanium (IV) oxide TiO_2, bismuth (III) oxide, Bi_2O_3, and barium carbonate $BaCO_3$ and Nd_2O_3 (0.5 wt%) by a conventional melt-quench technique.

Nd^{3+} doped ferroelectric BBiT glass-ceramics could be fabricated by melt-quenching and ceramization techniques. The material has a great potential for replacing the current generation of thin film ferroelectrics such as Lead Zirconia Titanates (PZT), both from an environmental point of view and to improve performance. The Glass transition temperature (T_g) of BBiT glass is about 475°C through DSC which is close to the value (480°C) through dilatometry. With increases in heating rates (α), T_g increases [33] and the glass stability factor has been found to lie within 150°C-160°C which indicates that the glasses are quite stable, having considerably high usage temperature.
The emission intensity of the $^4F_{3/2} \rightarrow {}^4I_{11/2}$ transition is enhanced by 9-fold with an increase in heat treatment time for 60 h compared to the precursor glass. The dielectric constant of glass-ceramic is about 18-53; however, it was found to increase with increases in the duration of heat treatment due to formation of more non-centrosymmetric ferroelectric crystals. Higher hardness of glass and GCs are obtained which are suitable for practical use [34].

CHAPTER 3
Experiment Details
3.1 Experimental Precursors

- Barium Acetate ($Ba(CH_3COO)_2$)
- Bismuth Nitrate ($Bi(NO_3)_3 \cdot 5H_2O$)
- Tetrabutyl Titanate ($Ti(OC_4H_9)_4$)
- Glacial Acetic Acid
- Ethanol
- Ethanolamine
- Acetyl Acetone

3.2 Experimental Apparatus

- Weighting Machine (Sartorius, BSA224-CW)
- Mortar and Pestle
- Flask
- Funnel
- Spatula
- Filter Paper
- Aluminium Boat
- Magnetic Stirrer (REMI, 2MLH)
- Ultrasonic Cleaner (PIEZO-U-SONIC)
- Tube Furnace

3.3 Experimental Procedure

In the experiment, Barium Acetate ($Ba(CH_3COO)_2$), Bismuth Nitrate($Bi(NO_3)_3 \cdot 5H_2O$) and Tetrabutyl Titanate ($Ti(OC_4H_9)_4$) were used as starting materials. The solvents chosen for this study were Glacial Acetic acid (CH_3COOH) and Ethanol (CH_3CH_2OH), while the complexation reagent used was Ethanolamine ($H_2NCH_2CH_2OH$), and the stabilizing agent employed was Acetylacetone ($CH_3COCH_2COCH_3$). The aim of this was to effectively stabilize Tetrabutyl Titanate. In order to prevent the excessive hydrolysis of $Ti(OC_4H_9)_4$, the 99% pure $Bi(NO_3)_3 \cdot 5H_2O$ was dried at 60°C for 8 hr. And then solved in Glacial Acetic acid. After the solution became transparent, they were mixed with $Ba(CH_3COO)_2$ acetum. Acetylacetone was used to stabilize Tetrabutyl Titanate, and then modified Tetrabutyl Titanate was added to the Bi-Ba acetum mixed solution with constant stirring at room temperature. To adjust viscosity, reduce the surface tension of the precursor and prevent the hydrolyzation of Bismuth nitrate in Acetic acid, Ethanolamine was added to the solution under ultrasonic agitation. In order to maintain a pH value of approximately 3.5, glacial acetic acid was utilized to perform the necessary adjustment. The resultant solution was filtered to form the stock solution, which was transparent, yellow and clear.

3.4 Calculation

3.4.1 Undoped Barium Bismuth Titanate

In Barium Bismuth Titanate $BaBi_4Ti_4O_{15}$, Ba, Bi and Ti are in the ratio 1:4:4. Barium will come from Barium Acetate, Bismuth from Bismuth Nitrate and Titanium from Tetrabutyl Titanate.

For 20 gm of Bismuth Nitrate-
Amount of Barium Acetate required =2.6298 gm
Amount of Tetrabutyl Titanate required =14.0213 gm

3.4.2 Iron doped Barium Bismuth Titanate

Iron will take place of Bismuth in Iron doped BBiT as follows $BaBi_{4-x}Fe_xTi_4O_{15}$ where x=0.05, 0.075 and 0.1

When x=0.05

We know 10 gm of $Bi(NO_3)_3 \cdot 5H_2O$ has 4.3082 gm of Bismuth or 0.0206 mole of Bismuth in it.
Now substituting x=0.05 we get $BaBi_{3.95}Fe_{0.05}Ti_4O_{15}$ which means ratio of Ba:Bi:Fe:Ti=1:3.95:0.05:4

Amount of Barium Acetate required =1.332 gm
Amount of Tetrabutyl Titanate required = 7.09948 gm
Amount of $Fe(NO_3)_3.9H_2O$ required = 0.1053439 gm

When x=0.075

x=0.075 gives $BaBi_{3.925}Fe_{0.075}Ti_4O_{15}$ which means ratio of Ba:Bi:Fe:Ti=1:3.925:0.075:4

Amount of Barium Acetate required = 1.34 gm
Amount of Tetrabutyl Titanate required= 7.1447003655 gm
Amount of $Fe(NO_3)_3.9H_2O$ required= 0.159 gm

When x=0.1

x=0.1 gives $BaBi_{3.9}Fe_{0.1}Ti_4O_{15}$ which means ratio of Ba:Bi:Fe:Ti=1:3.9:0.1:4

Amount of Barium Acetate required= 1.3491205 gm
Amount of Tetrabutyl Titanate required= 7.1904998102 gm
Amount of $Fe(NO_3)_3.9H_2O$ required= 0.2133906892 gm

3.5 Experimental Steps

- At first 20 gm Bismuth nitrate ($Bi(NO_3)_3 \cdot 5H_2O$) weighted at the weight machine.

Figure 8: Weighting Machine

- Bismuth nitrate ($Bi(NO_3)_3 \cdot 5H_2O$) was dried by air tight oven at 60°C for 8 hrs.

Figure 9: Hot Air Oven

- Then solved the dried Bismuth nitrate ($Bi(NO_3)_3 \cdot 5H_2O$) in glacial acetic acid using Magnetic stirrer.

Figure 10: Magnetic stirrer

- After the solution became transparent, it is mixed with Barium acetate ($Ba(CH_3COO)_2$), put solution in separate beaker known as Bi-Ba acetum mixed solution.

- Now take Acetylacetone and mix it with Tetrabutyl titanate to stabilize it against hydrolysis with constant stirring at room temperature.

- Then modified Tetrabutyl titanate is mixed with Bi-Ba acetum mixed solution with constant stirring at room temperature.

Figure 11: Modified Tetarabutyl tinate mixed with Bi-Ba acetum

- Ethanolamine was added to adjust viscosity, reduce surface tension and prevent hydrolyzation in above solution under Ultrasonic Agitation**.**

- To control pH (about 3.5) Glacial Acetic acid is also added.

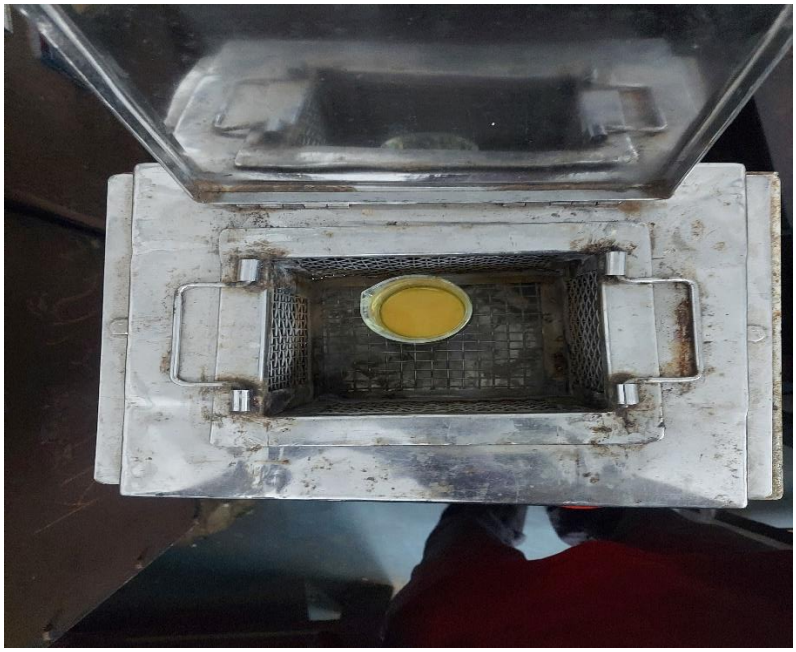

Figure 12: Ultrasonic Agitation

- The solution was in ultrasonic agitation for 30 minutes.
- Ater ultrasonic agitation the resultant solution was filtered out using filter paper in conical flask to separate out yellow substance on filter paper and it was collected in Aluminium Boat.

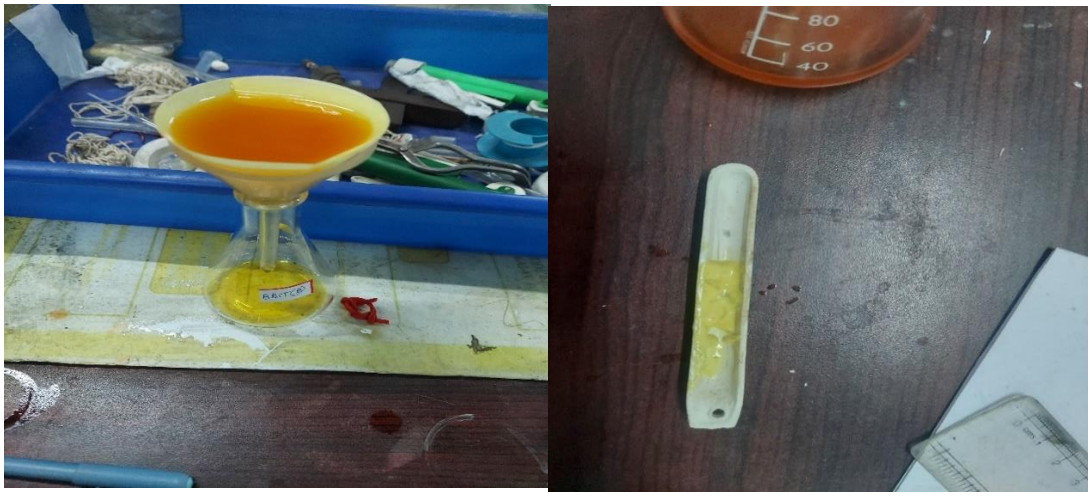

Figure 13: Filter paper and Aluminium boat

- Alumina boat is put inside tube furnace for heat treatment at different temperature.

- After heat treatment, dried part was collected in Morter and Pestle and made it fine powder.

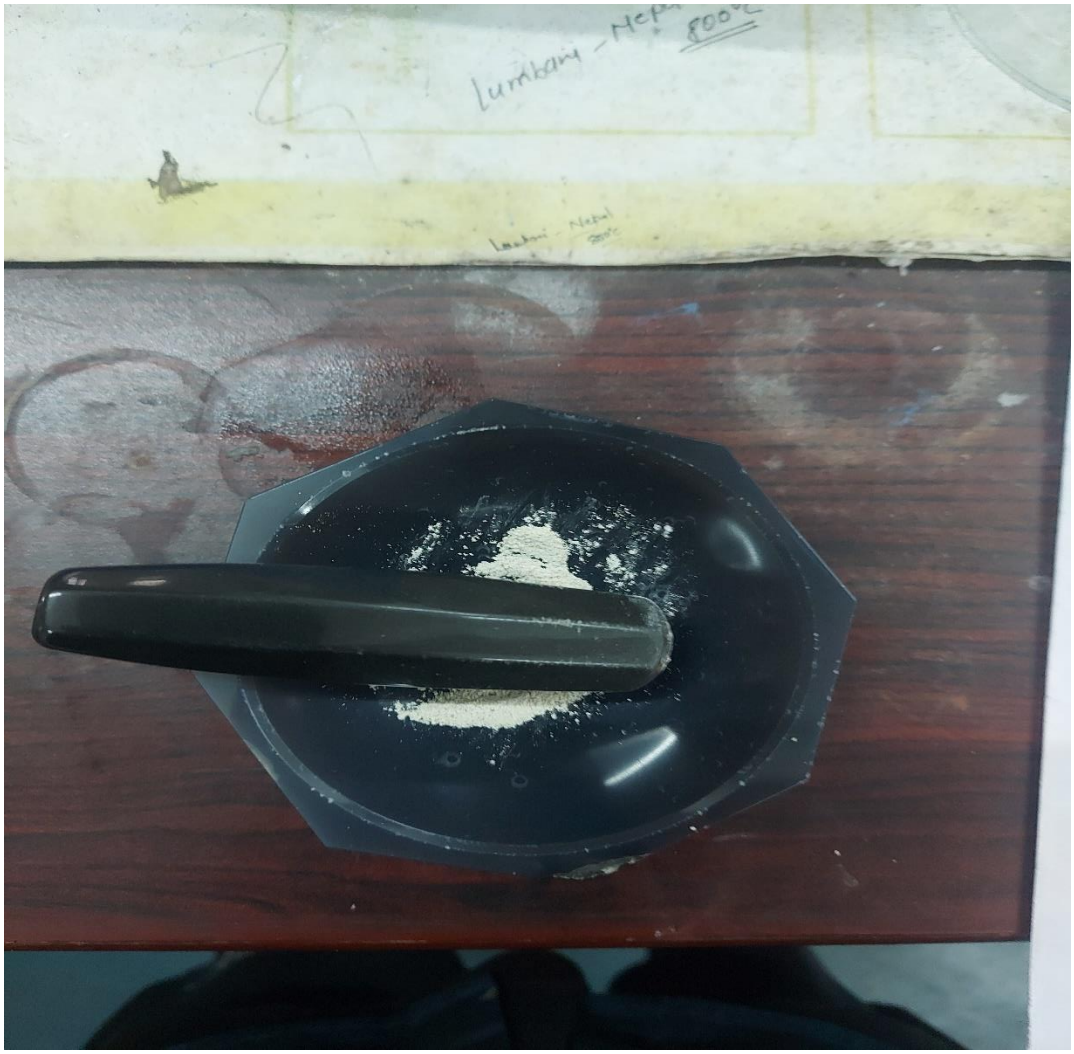

Figure 14:Morter and Pestle

3.6 Tube Furnace

A tube furnace serves as an electrically operated heating apparatus that facilitates the processes of inorganic compound synthesis and purification, whilst also being intermittently employed in organic synthesis. A plausible design involves the integration of heating coils in the form of a spring within a ceramic tube. This configuration is capable of withstanding a continuous temperature of up to 1200ºC within a thermally insulated chamber. The regulation of temperature is achieved through the utilization of feedback information obtained from a thermocouple [35].

At temperatures exceeding 1200 degrees Celsius, a ceramic tube located within an insulated chamber is subject to heating via rod or U-shaped heating elements made of silicon carbide. Such a furnace is capable of withstanding temperatures as high as 1500 degrees Celsius. Advanced heating elements comprising molybdenum disilicide, available in select models, have the capability to attain operational temperatures of up to 1800°C.

Elaborate tube furnaces often possess multiple heating zones, allowing for effective transport experimentation and the attainment of a more homogenous heat distribution within the central region of the furnace. Several digital temperature controllers feature an RS232 interface that allows the user to program segments for various applications, including but not limited to, ramping, soaking, and sintering. This enables the implementation of more complex and advanced applications. The materials often employed for the reaction tubes comprise of alumina, Pyrex, and fused quartz.

Common uses of tube furnaces are brazing, sintering, synthesis, tempering, calcination, degassing etc. [36]

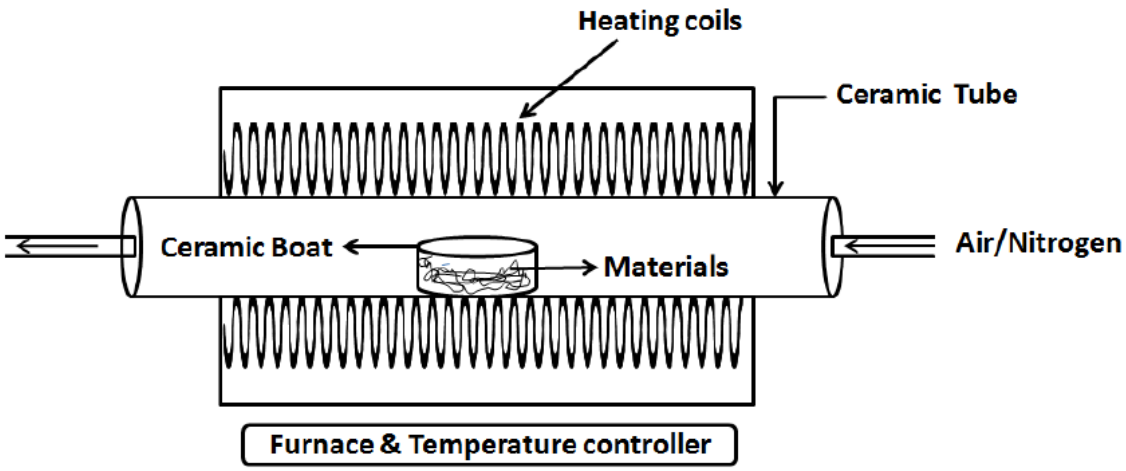

Figure 15: Schematic of Tube Furnace

Figure 16: Tube Furnace

CHAPTER 4

Characterization Process

4.1 X-Ray Diffraction Spectroscopy (XRD)

X-ray diffraction (XRD) is a versatile, non-destructive technique that reveals detailed information about crystallographic structure of natural and manufactured materials. It is routinely used for phase identification and determination of unit cell dimensions. Crystalline substances behave as three-dimensional diffraction gratings for X-rays having wavelengths similar to the spacings of planes in a crystal lattice. X-rays, when fall on crystals undergo diffraction. When the X-ray wave length (λ) and plane spacings (d) satisfy the Bragg condition 2d sin θ = n λ constructive interference in the diffracted rays occur and a peak in the intensity in observed. A recording of this intensity as function of 2θ is what is called X-ray diffraction pattern (2θ is the angle between diffracted and undiffracted beam) and contains number of sharp intensity peaks for crystalline materials. This pattern is analysed and information about spacing 'd' and related crystal structure is obtained [37].

The geometrical interpretation of XRD phenomena is given by Bragg's law- $2d\ sin\theta = n\lambda$ where, d = Lattice spacing(nm) θ= Diffracted beam angle (in degree) n= order of diffraction. λ = x-ray wavelength

To calculate the crystallite size using XRD data, the Debye Scherrer equation can be employed.

Crystallite size, $$d = k\lambda/\beta cos\theta$$

where, d is the dimension(measured) of the particle in the direction perpendicular to the reflecting plane

k= Scherrer constant (crystallite shape factor with approximate value of 0.9),

λ= wavelength of the used X-ray beam (1.54184 Å or 0.154184nm),

β= Full width at half maximum (FWHM) of the peak expressed in radian, and

θ= Bragg diffraction angle.

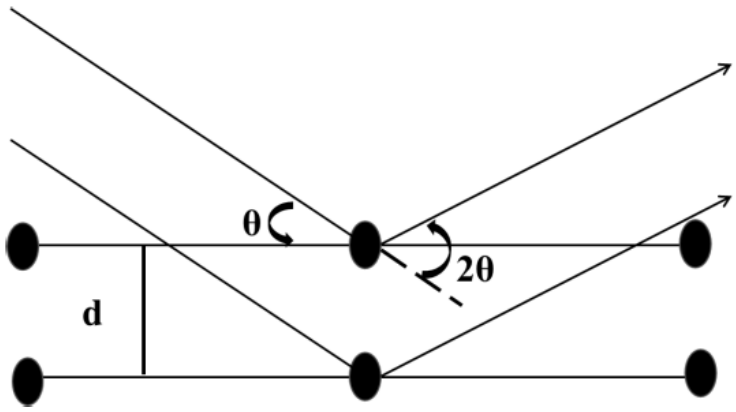

Figure 17: Principal of XRD

Figure 18: SmartLab SE XRD set up

4.2 TG-DTA

Thermal gravimetric analysis (TGA) is a thermal analysis method that characterizes variations in physical and chemical traits of materials with respect to increasing temperature, while maintaining a constant heating rate or constant temperature and/or constant mass loss as a function of time. In TGA, a small amount of specimen is heated in an inert or reacting atmosphere, and any resulting mass changes are measured with respect to temperature. TGA is done to determine specific properties of materials that display mass loss or gain owing to decomposition, oxidation, or volatile loss (such as moisture) [38]. Few common applications of TGA are-
material characterization by analysing characteristic decomposition patterns, investigating degradation mechanisms and reaction kinetics, estimation of the amount of organic and inorganic material in a sample which could be used as a chemical analysis or to confirm predicted material structures, determining thermal stability, oxidative stability, chemical composition, and water content in a sample material.

The x-axis in a TGA curve stands for the temperature (or time, and frequently a direct heating rate), and the y-axis the percentage of mass loss. This technique has been used to characterise different metal oxide samples including BBiT [39].

Phenomena causing mass changes-
1) Physical

- Gas adsorption
- Gas desorption
- Phase transitions

- Vaporization
- Sublimation

2) Chemical
- Decomposition
- Break down reactions
- Gas reactions
- Chemisorption (adsorption using chemical forces rather than physical ones)

Differential thermal analysis (DTA) is an important characterization tool to determine heat change measurements and whether the process and endothermic or exothermic. decomposition behaviour in various atmospheres.
phase diagrams

The Differential Thermal Analysis (DTA) technique entails the measurement of the temperature variation between a reference and a specimen due to a predetermined quantity of heat input. Here, ΔT signal is referred to as the DTA signal α-alumina is used as reference material in DTA. The combined application of TGA-DTA techniques is advantageous as it allows for the comprehensive determination of a sample's thermal properties within the context of a single experimental run.

Phenomena causing changes in heat /temperature-

1) Physical
- Adsorption (exothermic)
- Desorption (endothermic)
- A modification in the crystalline arrangement (resulting in either an endothermic or exothermic effect)
- Crystallization (exothermic)
- Melting (endothermic)
- Vaporization (endothermic)
- Sublimation (endothermic)

2) Chemical
- Oxidation (exothermic)
- Reduction (endothermic)
- Break down endothermic or exothermic reactions
- Chemisorption (exothermic)
- The phenomenon of solid-state reaction, which can be either endothermic or exothermic

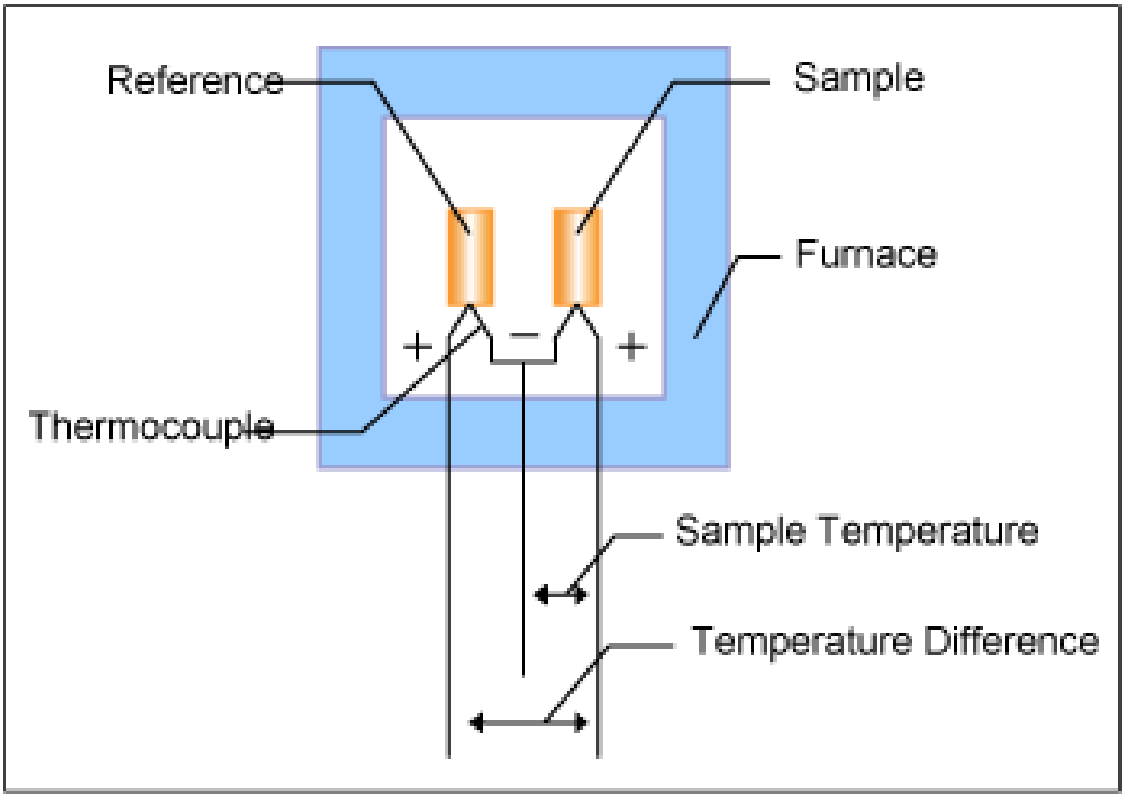

Figure 19: Block diagram of DTA

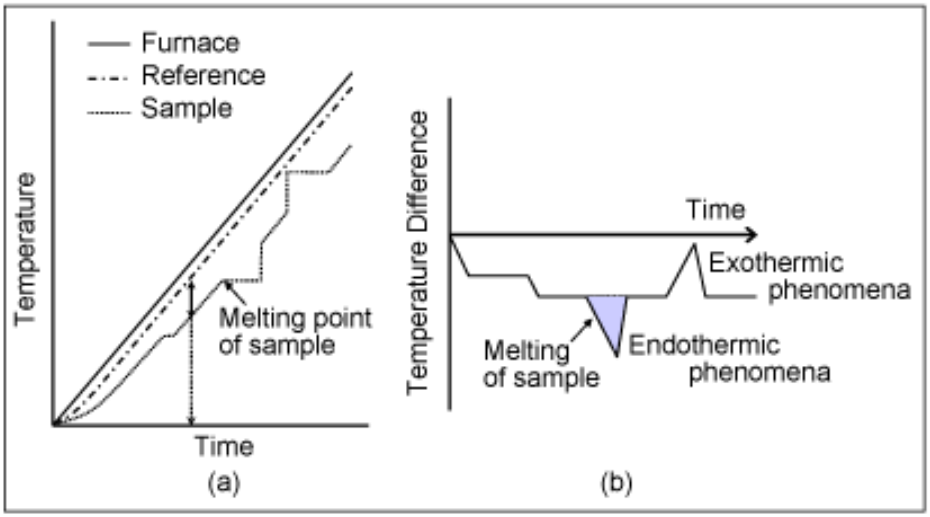

Figure 20: Measurement principles of DTA

4.3 FESEM and EDX

FESEM is used to study the morphology of the synthesized BBiT with an accelerating voltage about 30.0 kV. From the FESEM imaging we can obtain information about the shape, the size distribution, and dimensions of the given samples. The FESEM is composed of electron source, electromagnetic lenses, and electron detector. The lenses on the sample's surface accelerate and focus a highly energetic electron beam. Then the sample emits secondary electrons which can be detected [40]. The emitted secondary electrons number are varied due to the surface variation of the sample. The SEM image

is created by scanning the beam over the surface of the sample in a raster way and detecting the variation of electrons number that emitted from the surface of the sample as shown in the schematic diagram. Another interaction is that the electron beam can ionize the atoms, and x-ray emitted, which depend on the elemental composition of the sample. Also, by scanning the surface of the sample and detecting the x-ray with another detector, chemical composition and their distribution over the sample which is known as energy dispersive x-ray (EDX) could be analysed [41]. Therefore, from the SEM we can obtain a magnification image of the surface of the sample as well as the chemical composition.

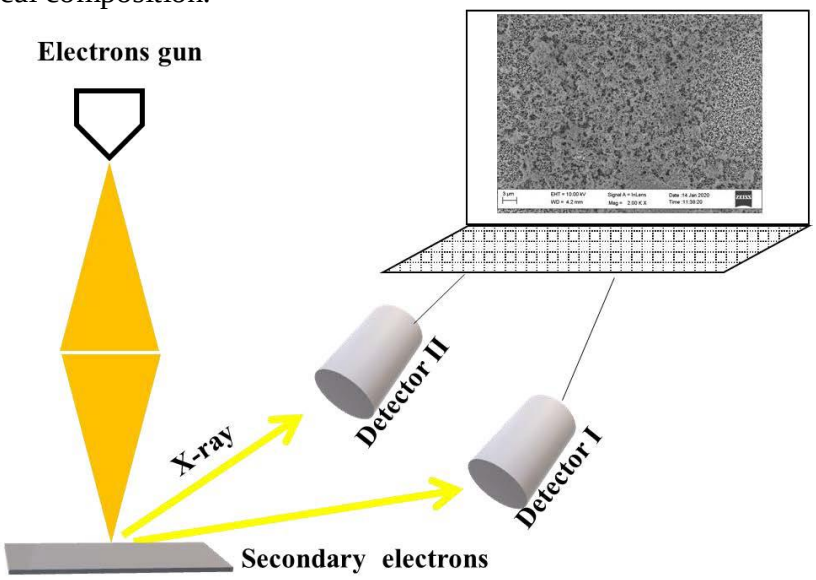

Figure 22: Schematic diagram of the SEM

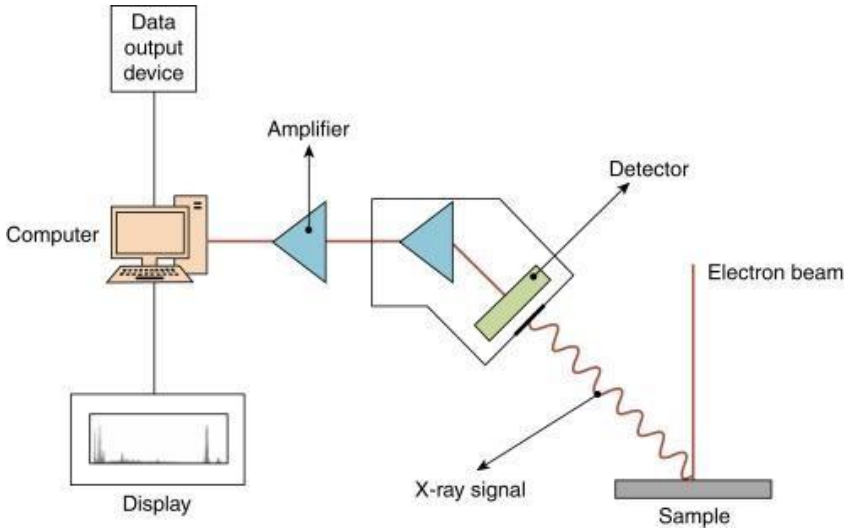

Figure 21:EDX Process Outline

4.4 FTIR

The widely utilized approach for infrared spectroscopy is designated as Fourier Transform InfraRed (FTIR). In the field of infrared spectroscopy, a sample is subjected to IR radiation, allowing for analysis and characterization of its molecular structure and properties. A portion of the infrared radiation is assimilated by the specimen while the remaining fraction is transmitted through it. The spectrum that emerges is an indication of the molecular absorption and transmission characteristics of the sample, thus leading to the development of a molecular fingerprint. Similar to a fingerprint, the infrared spectrum is distinct for each molecular structure, thus highlighting the uniqueness of such structures. The efficacy of infrared spectroscopy renders it application in various analytical methodologies [42].

Information FTIR can provide-

- It can identify unknown materials
- It can establish a sample's consistency or quality. It can calculate the proportion of each ingredient in a mixture

The utilization of infrared spectroscopy has been extensively employed as a fundamental approach for the evaluation of materials in laboratory settings for a considerable period spanning over seven decades. The infrared spectrum of a given sample constitutes a distinct identifier characterized by considerable absorption peaks that correspond to the frequencies of bond vibrations among the constituent atoms comprising the material. Due to the fact that every distinct material consists of a distinctive configuration of atoms, there are no two compounds that yield an identical infrared spectrum. Consequently, it can be inferred that infrared spectroscopy has the potential to provide a definitive recognition (qualitative scrutiny) of all dissimilar modes of matter. Furthermore, it should be noted that the magnitude of the peaks observed in the spectrum furnishes a straightforward and unequivocal indication of the quantity of substance that is currently available. The utilization of contemporary software algorithms has enabled infrared spectroscopy to be a proficient tool for carrying out quantitative analyses [43].

Advantages of FTIR-

- **Speed:** The expeditious nature of Fourier transform infrared (FTIR) measurements is attributable to the simultaneous measurement of all frequencies. As a result, most assessments conducted via FTIR require mere seconds to complete, rendering the technique markedly faster than traditional methods which may necessitate several minutes for completion. This phenomenon has been commonly characterized as the Felgett Advantage.
- **Sensitivity:** The utilization of Fourier transform infrared (FT-IR) technique yields a notable enhancement in sensitivity for numerous reasons. The measurement apparatus utilized in this study exhibits heightened levels of sensitivity, with concurrently elevated values of optical throughput (commonly referred to as the Jacquinot Advantage). As a direct result of these characteristics, the apparatus possesses significantly decreased levels of noise interference. Furthermore, rapid scanning capabilities are integrated into this apparatus, allowing for the integration of multiple scans in order to reduce measurement noise to customized levels (termed signal averaging).
- **Mechanical Simplicity:** The interferometer's moving mirror is its only

continuously moving component.

- **Internally Calibrated:** Internally calibrated: In accordance with the Connes Advantage, the devices use a HeNe laser as an internal testing reference for wavelength measurement. These instruments possess self-calibration capabilities, therefore no need to calibrate by user [44].

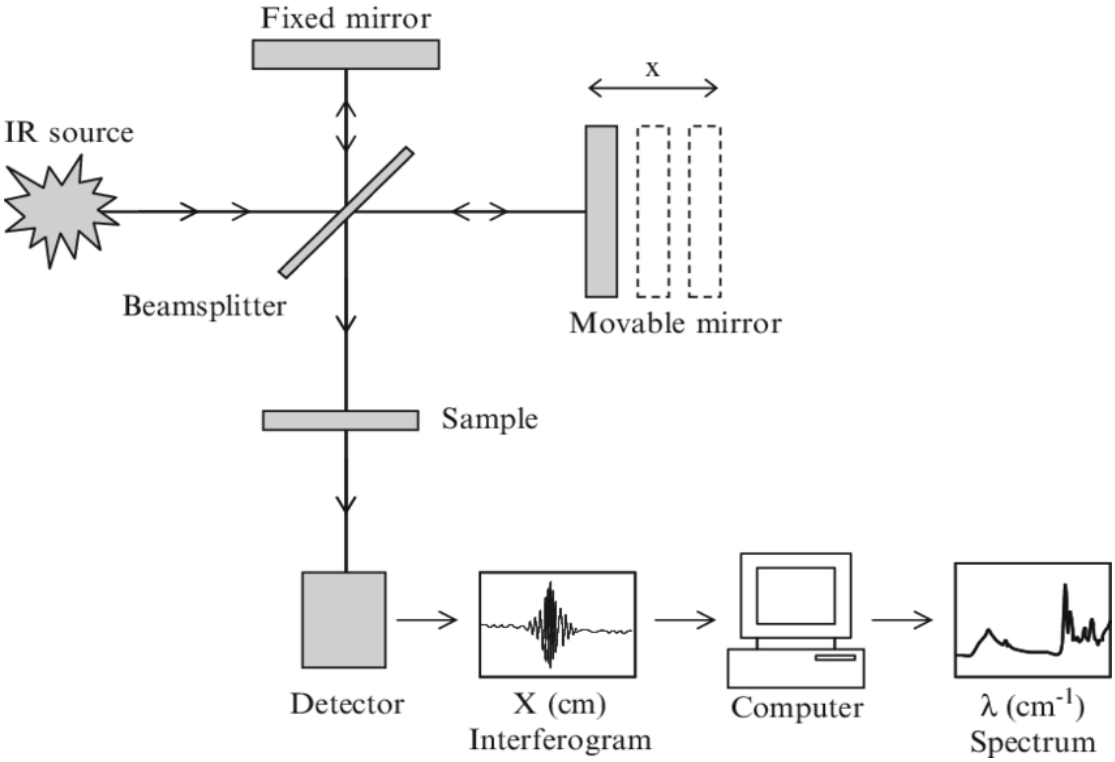

Figure 23: Schematic diagram of FTIR spectrometer

4.5 Photoluminescence

4.5.1 Photoluminescence: Light matter interaction

Photoluminescence spectroscopy works in a non- contact mode. The aforementioned is a non-invasive methodology employed to investigate the electronic configuration of materials.

When a sample is exposed to light, it undergoes a process of absorption wherein the excess energy of the light is transferred to the material through a phenomenon called photoexcitation. One manner in which sample dissipates this excess energy is through light emission, i.e., luminescence. In the event of excitation through photon absorption, the phenomenon of luminescence is recognized as photoluminescence in the academic context.

Excitation causes material's electrons to occupy the allowed excited states. These excited electrons return to their stable position, i.e., equilibrium or ground state by dissipating the extra energy in the form of either light known as radiative process or by any non-radiative process. The emitted light energy (photoluminescence) is linked with the energy difference in energy of the two electronic states taking part in the transition between the excited and equilibrium states. The radiative process component determines the magnitude of light that is emitted [45].

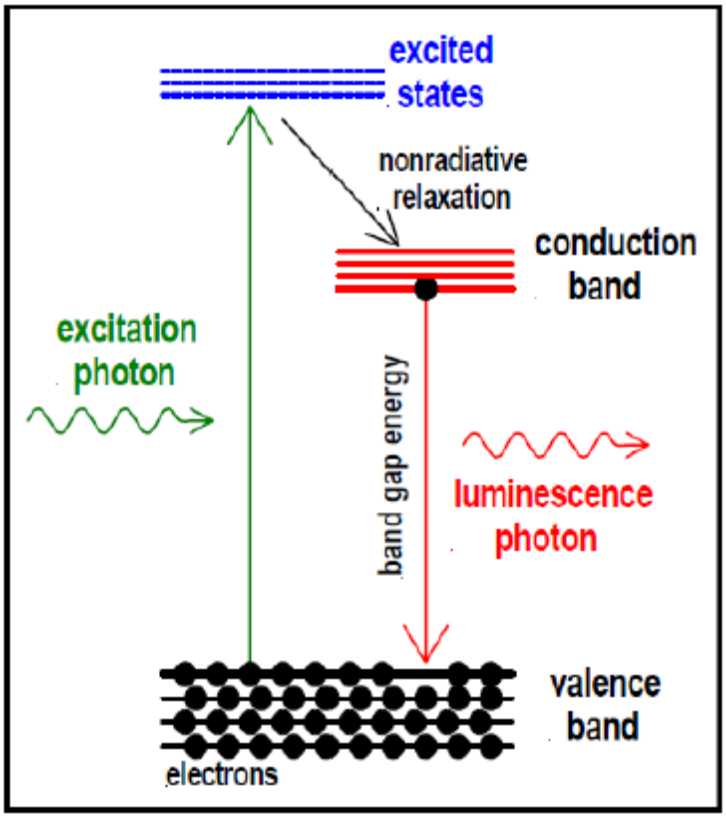

Figure 24: Principle of Photoluminescence spectroscopy

4.5.2 Relation between absorption and emission spectrum

At reduced energy levels, the likelihood of fluorescence and phosphorescence surpasses that of absorption (excitation energy). As presented in Figure 26 , in case of absorption, λ_0 wavelength means transition from the ground state of vibration i.e., S_0 to S_1. When absorbing radiation, S_1 molecule which excited vibrationally goes to lower vibrational level before emitting any radiation. λ_0 wavelength corresponds to transition of very high energy, cascade of peaks occur at higher wavelength. Both emission as well as absorption spectrum are likely to have mirror image relation if spacing of vibrational levels are approximately equivalent and if the probability of transition is alike. Figure , λ_0 transitions do not overlap completely. As illustrated in Figure #, a molecule with radiation absorption properties that predominantly exists in its ground state, S0, exhibits a stable molecular structure alongside solvation. The transitions in the electronic states are rapid in comparison to atoms vibrational movement or the solvent molecules' translational movement, once the radiation is absorbed, the S_1 excited molecule yet have its geometry as well as solvation S_0 state. The level of geometric and solvation alterations is substantially adjusted after excitation. This rearrangement lowers the energy of excited molecule. When an S_1 molecule fluoresces, it returns back to the S_0 state having S_1 geometry and solvation. The aforementioned unbalanced configuration is expected to possess a greater energy level compared to an S0 molecule exhibiting S0 geometry and solvation. The net outcome has been shown in Figure in which excitation energy is higher than the emission energy [46] [47].

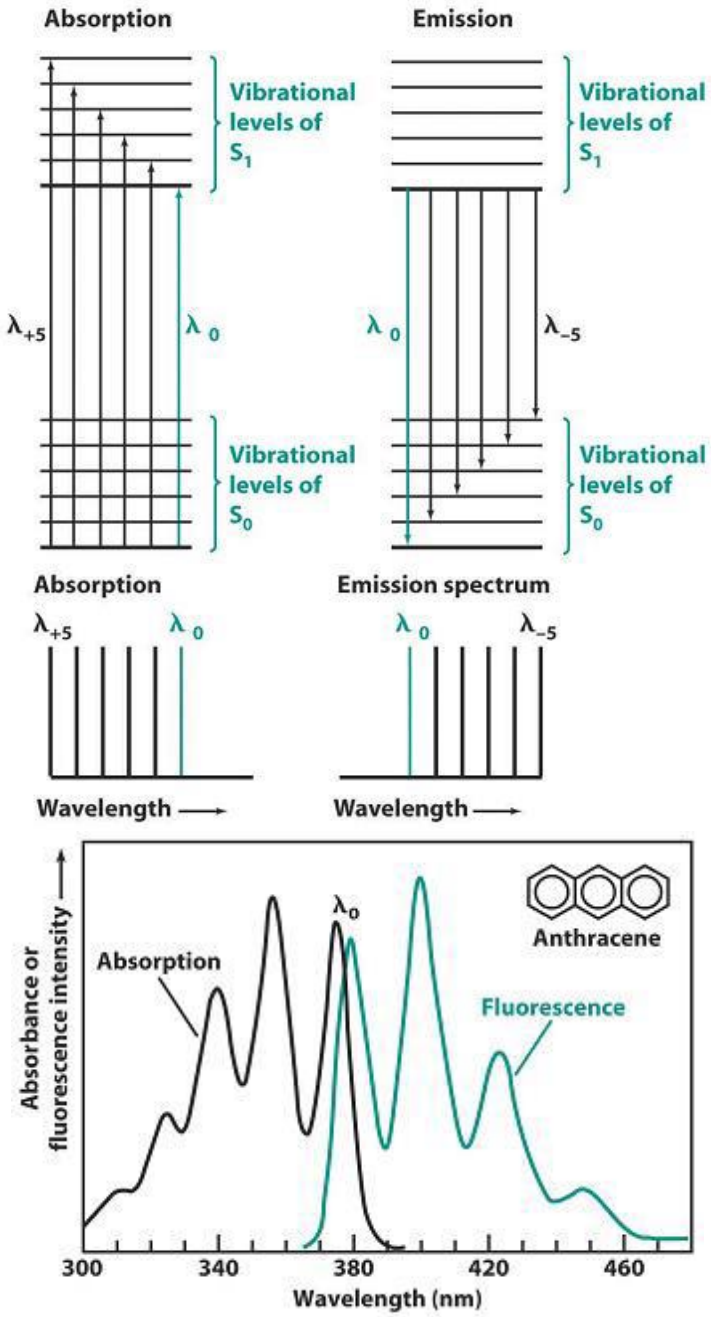

Figure 25: Energy level diagram and Emission and excitation spectra

4.5.3 Limitations

Even though this method lacks quality, it can still be used to find optical centres that are sparsely distributed. The major scientific PL limitation is that several optical centres might possess numerous excited states that are vacant at low temperatures.
One significant constraint of photoluminescence (PL) is the loss of luminescent signal. In the characterization centres of silicon, specifically those used in PL experiments, it has been observed that the presence of self-interstitials results in the absence of sharp-line PL emanating from the 969 meV centres [48].

CHAPTER 5
Result And Discussion

5.1 XRD Analysis

XRD studies were performed on 3 undoped sample and 3 Iron doped samples. Undoped samples were heat treated at different temperature and time namely, Sample A=600°C for 4 hours, Sample B=500°C for 5 hours and Sample C=550°C for 6 hours. XRD confirms the phase development after annealing at 600°C for 4 hours, 500°C for 5 hours and 550°C for 6 hours as per JCPDS card no 8-261. Amongst them 500°C for 5 hours (Sample B) yield the best result for phase development with all peaks got indexed as per planes from JCPDS. The other two yield some minor impurity phase but the major peaks got indexed as per planes of thermodynamic feasibility confirming the formation of barium bismuth titanate.
Since Sample B is the purest out of 3 samples therefore doped samples were heat treated for same temperature and time as of Sample B.

5.1.1 XRD graphs of Undoped Samples

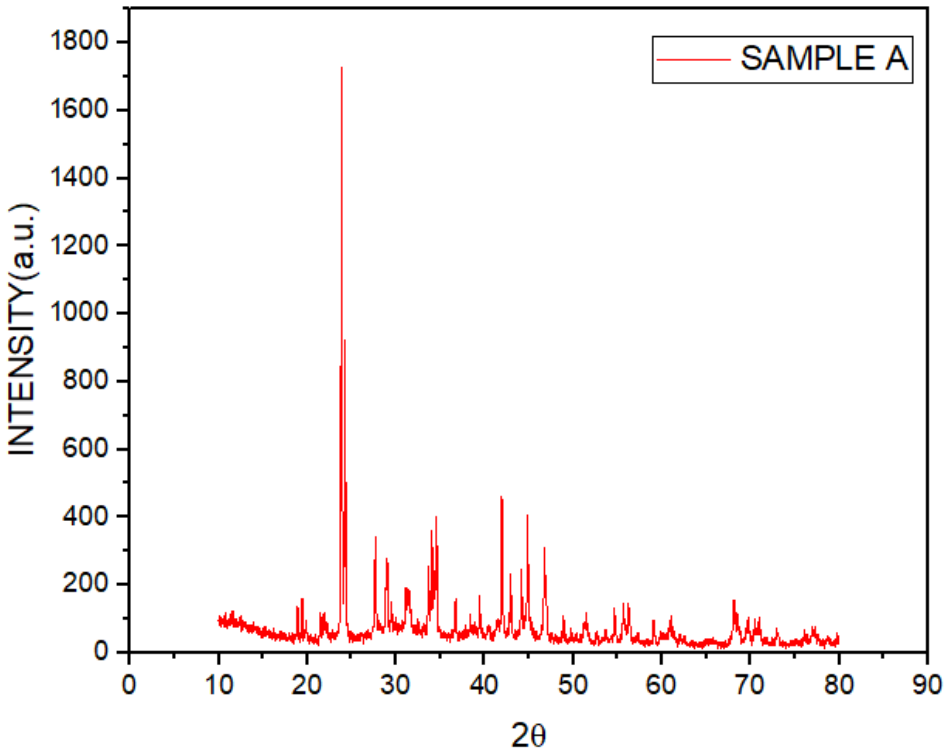

Figure 26: Sample A(600°C, 4 Hours)

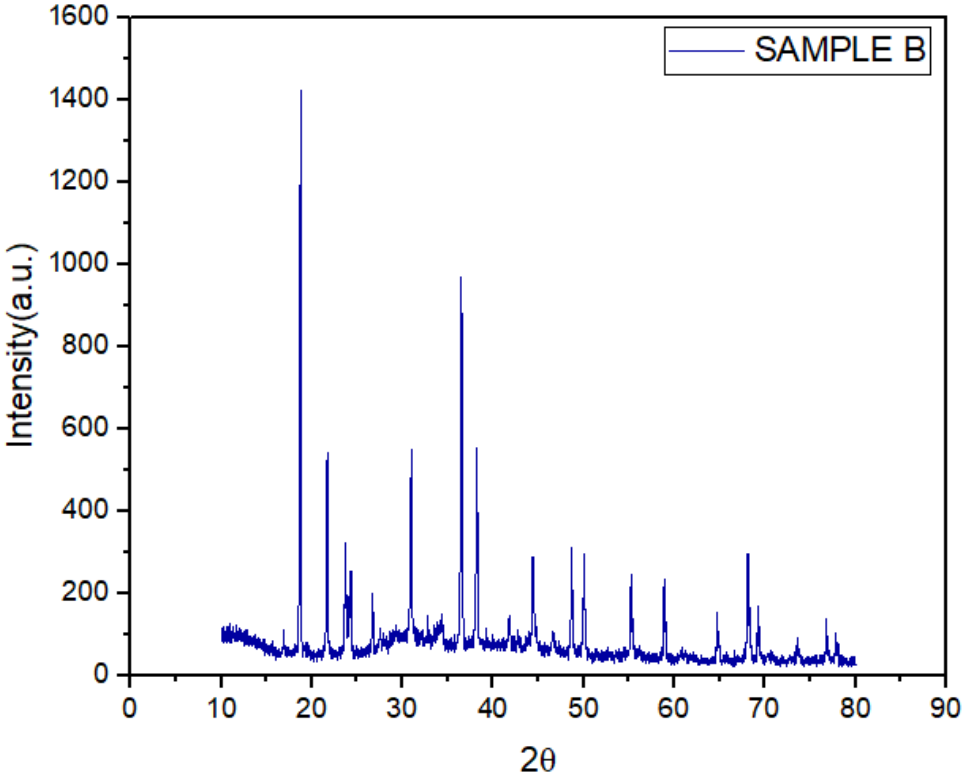

Figure 27: Sample B(500°C, 5 hours)

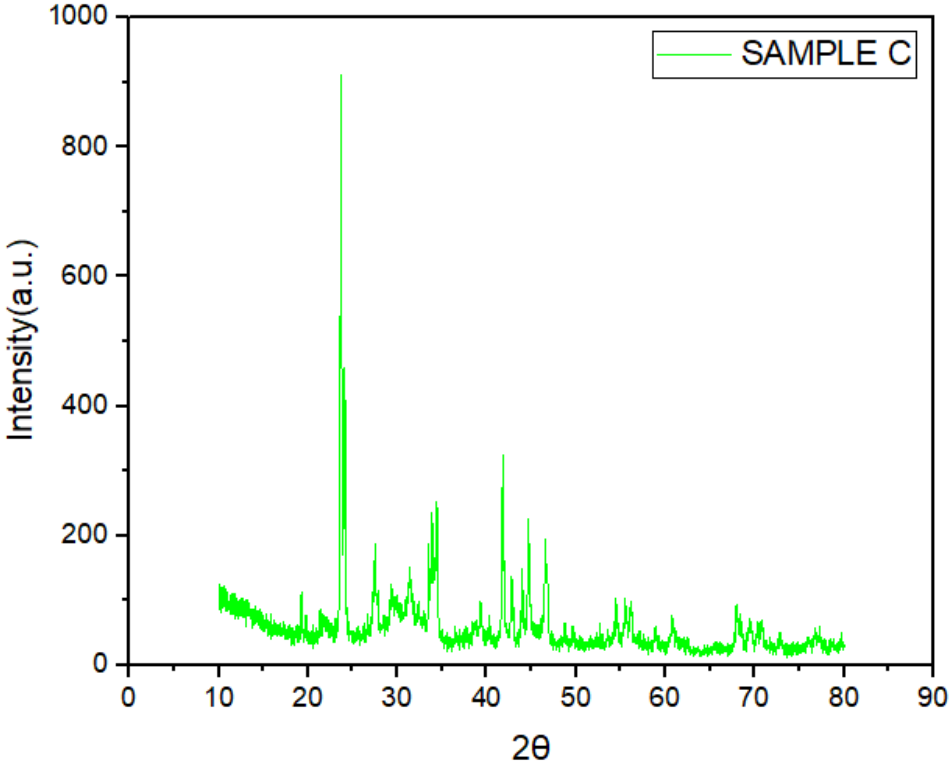

Figure 28: Sample C(550°C, 6 hours)

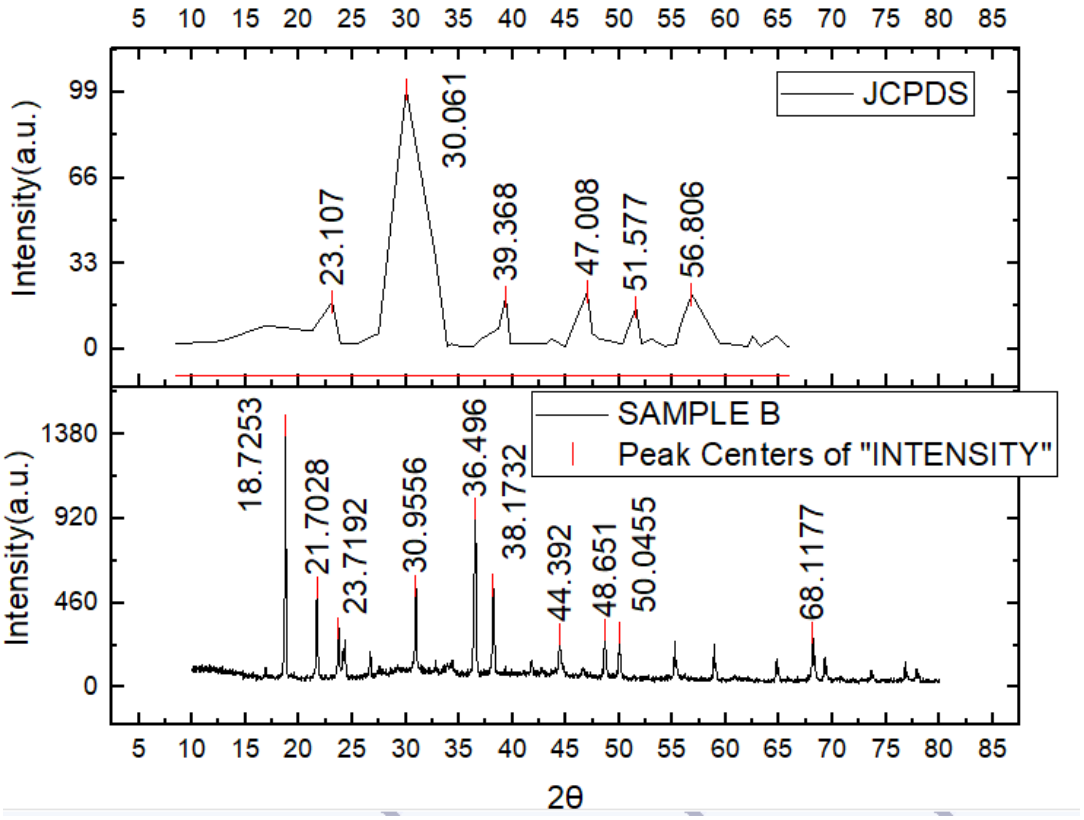

Figure 29: Sample B with JCPDS file

5.1.2 XRD graphs of Iron doped Barium Bismuth Titanate

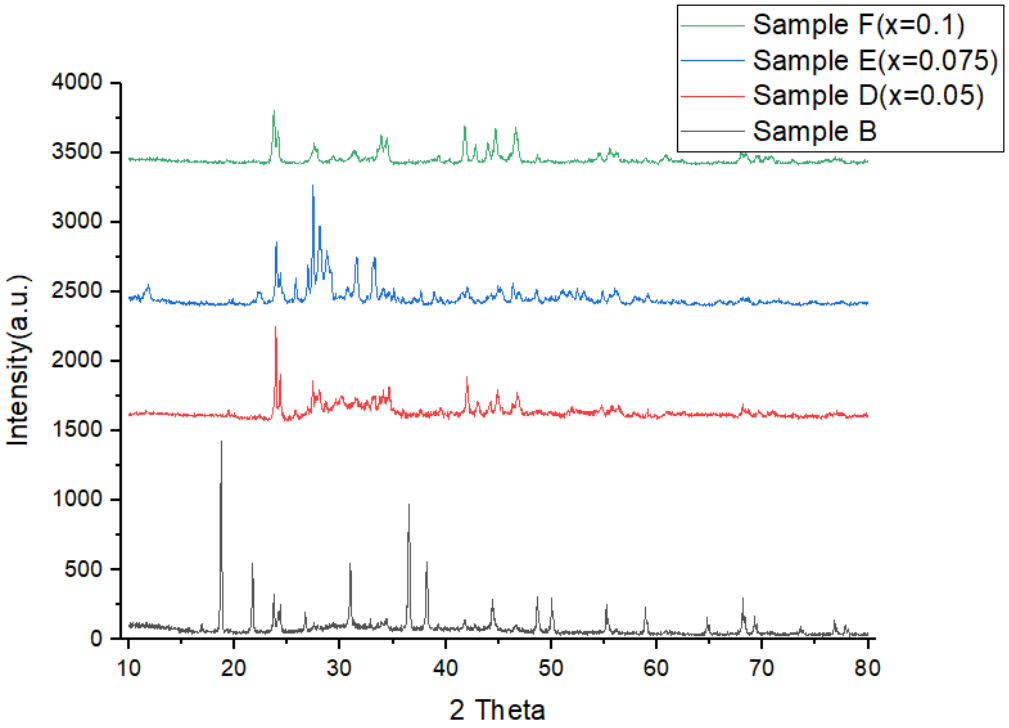

Figure 30: Undoped and doped sample's XRD

On doping XRD peaks either shift to lower angle or higher angle depending upon the substituted element. In case of interstitial doping where the doping element is larger in size peaks get shifted to lower angle because of tensile stress caused by larger doping element on the neighbouring atoms. While in case of substitutional doping where

doping element is smaller in size it causes compressive stress results in peaks shift to higher angle [49].

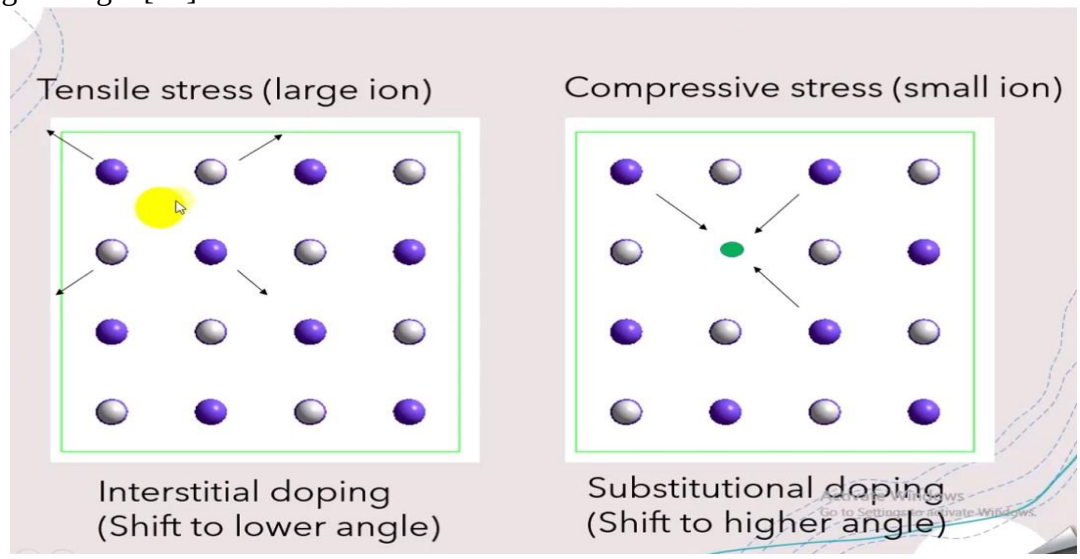

Figure 31: Effect of Doping

In our experiment doping element Iron(Fe) having atomic radius 126 pm is smaller than Bismuth having atomic radius 207 pm therefore peaks got shifted to higher angle as can be seen from the above XRD graph.

5.1.3 Crystallite Size

Scherrer formula is used to calculate the crystallite size of all the samples.

Sample	Crystallite Size(nm)
A	40.08
B	42.05
C	29.19
D	23.85
E	17.87
F	16.61

Table 2: Crystallite Size

Crystallite size of sample B is 42.05 nm which is purest sample among undoped samples. Crystallite sizes of samples D, E and F are 23.85 nm, 17.87 nm and 16.61 nm. We can clearly see that as the concentration of Iron increases in the sample (from x=0.050 to 0.1) crystallite sizes decreases because doped element is smaller in size than Bismuth whose Iron replaces [50].

5.1.4 Crystal Structure

From JCPDS data book we know that crystal system of Barium Bismuth Titanate is Tetragonal with space group 14/mmm.
Values of crystallographic constants are a=b=3.8624 Å and c=41.851 Å. α=β=γ=90°

We can verify the crystal system of BBiT using the following equation of interplanar spacing for a Tetragonal unit cell [51]- $\frac{1}{d^2} = \frac{h^2+k^2}{a^2} + \frac{l^2}{c^2}$

Where h,k and l is the miller indices, d is interplanar spacing, a and c are the lattice constant of unit cell.

d can be calculated by the Bragg's law given by- $n\lambda = 2dsin\theta$

In sample B, miller indices corresponding to peaks of 2ϴ angles 21.69283and 30.95601 are (0 0 10) and (1 1 0).

On calculation we get c=40.93486 Å and a=b=4.0832044. (See appendix 2)

Lattice constant	Standard values (Å)	Calculated values (Å)
a=b	3.8624	4.0832044
c	41.851	40.934860

Table 3: Lattice constants value

So calculated values are in very good approximation to standard values [52]. Therefore, we can surely say that the synthesized powder sample B is Barium bismuth titanate having tetragonal crystal system.

5.2 FTIR

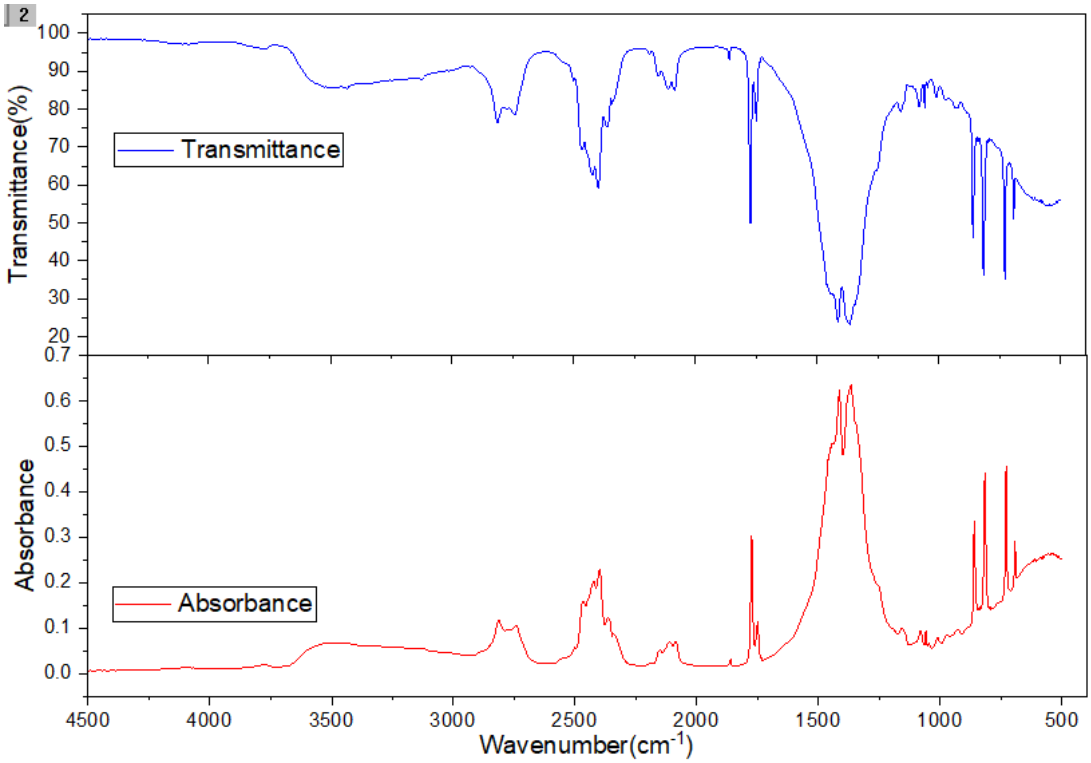

Figure 32: FTIR of Undoped sample

FTIR analysis is carried in the scan range of 500-4000 cm^{-1} using KBr as reference. The spectra positions at about 800-1100 cm^{-1} are due to Si-O-Si bond. Bending vibration of Si-O-Si bond is noted at about 860 cm^{-1} while those close to about 950 cm^{-1} is possibly for symmetric stretching vibration of Si-O bonds. The spectra within 480-680 cm^{-1} are attributed to Bi-O bonds while those around 730-750 cm^{-1} corresponds to asymmetric stretching of Ti-O tetrahedral units.

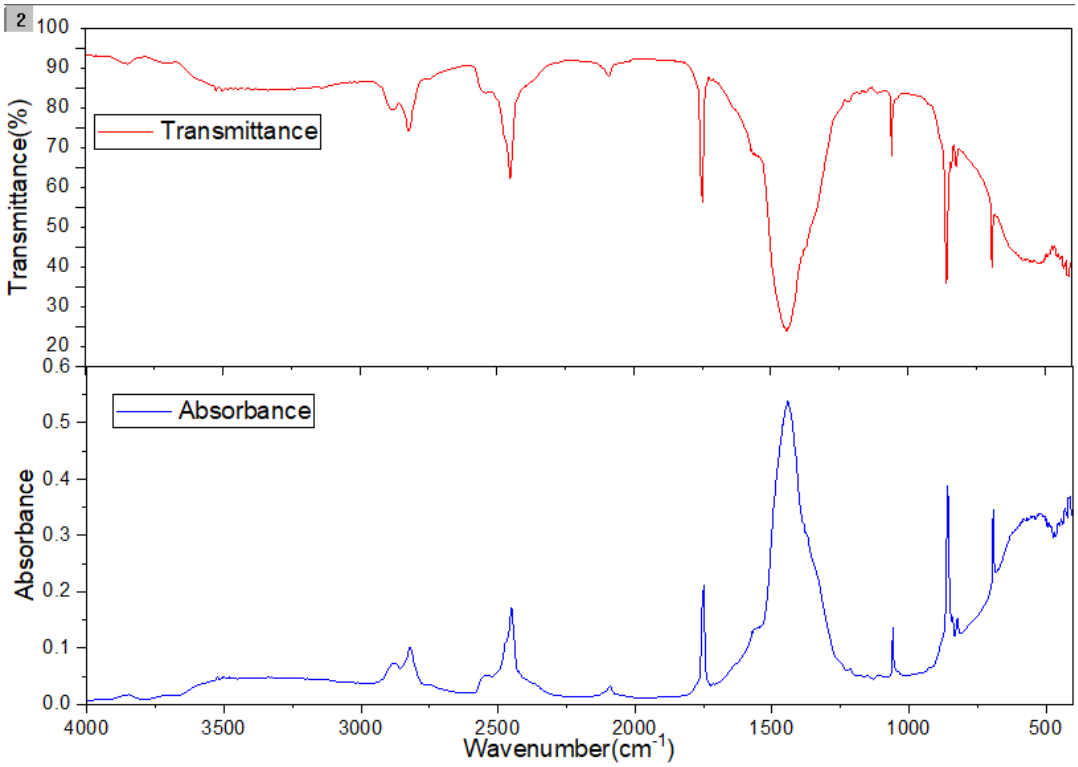

Figure 33: FTIR of Iron Doped Sample

FTIR spectra analysis of doped barium bismuth titanate is carried using KBr as reference. The peaks at positions about 860 and 1060 cm^{-1} are due to Si-O-Si bond. The strong band below 700 cm^{-1} is because of Fe-O stretching bond which is because Iron is doped into barium bismuth titanate and it replaces bismuth and make bond with oxygen [53]. Bending vibration of Si-O-Si bond is noted at about 860 cm^{-1}. While those close to about 950 cm^{-1} is possibly for symmetric stretching vibration of Si-O bonds. The spectra within 480-680 cm^{-1} are attributed to Bi-O bonds while those around 730-750 cm^{-1} corresponds to asymmetric stretching of Ti-O tetrahedral units [54].

5.3 TG/DTA

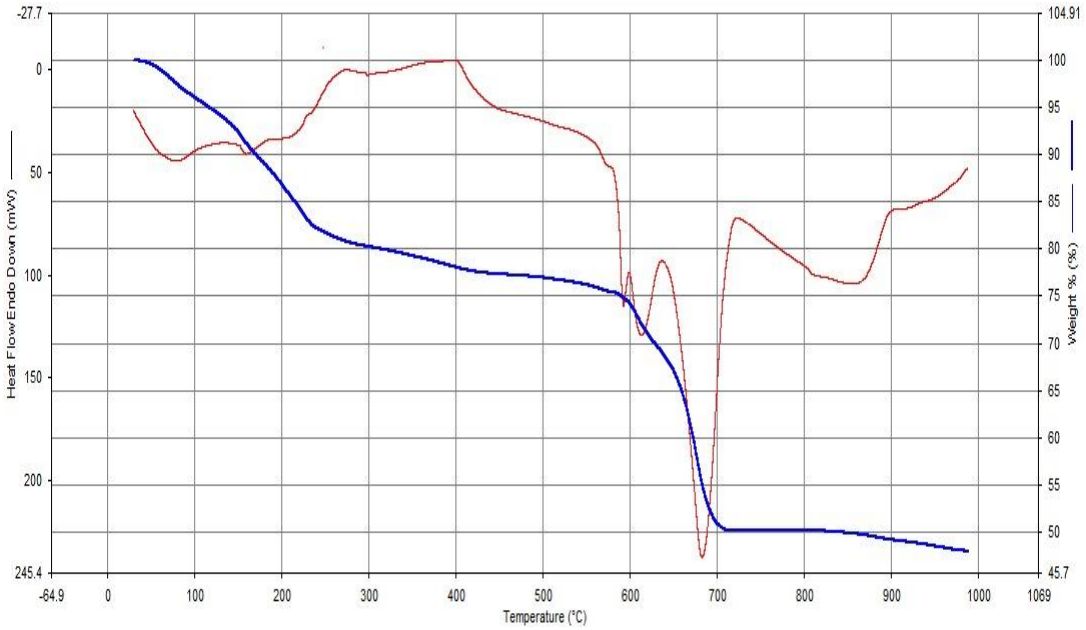

Figure 34: TG-DTA curve of Barium Bismuth Titanate synthesized at 500°C for 5 hours

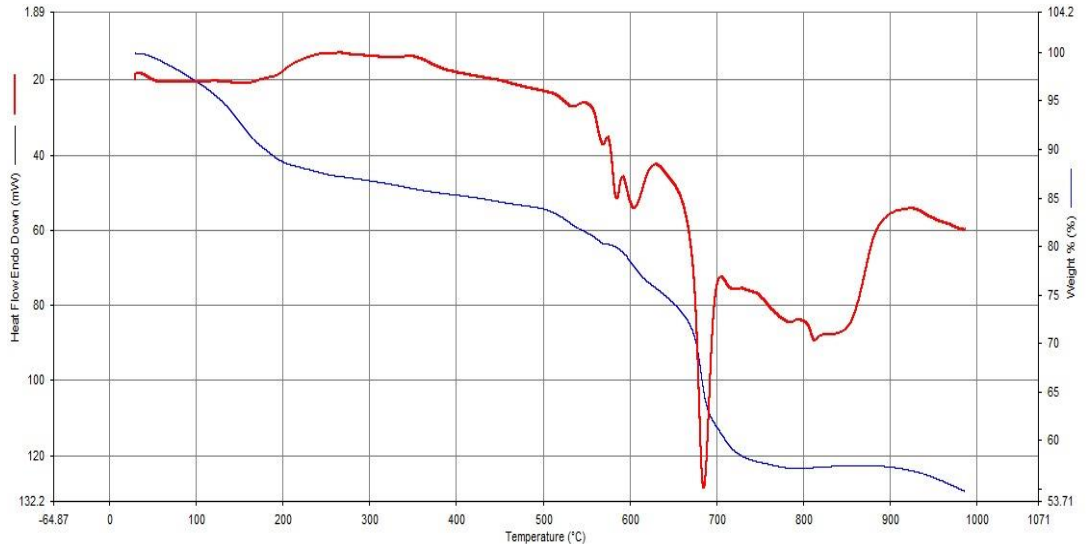

Figure 35: TG-DTA curve of Barium Bismuth Titanate synthesized at 600°C for 4 hours

Thermal analyses of two samples of Barium bismuth titanate heat treated at different temperature and time is carried to determine the crystallization of ceramics. Thermal analyses are carried in presence of nitrogen atmosphere till 1000°C. 3 endothermic peaks at about 5800-650°C and 700-720°C respectively while exothermic hump centered at about 880°C is noted. Prominent weight losses are noted at 100-200°C which is about 7-14 wt% due to desorption of physically adsorbed water(Dehydration phenomena) and chemisorbed water (Dehyroxylation phenomena) while another in the range 500-700°C which is almost about 27-30 wt% which can be attributed to the formation and crystallization of BBiT phase. Weight losses are found to diminished at around 800°C onwards. Thus, crystallization range is noted to be around 800°C for proper phase development of the material from precursors [55].

5.4 Photoluminescence Spectroscopy

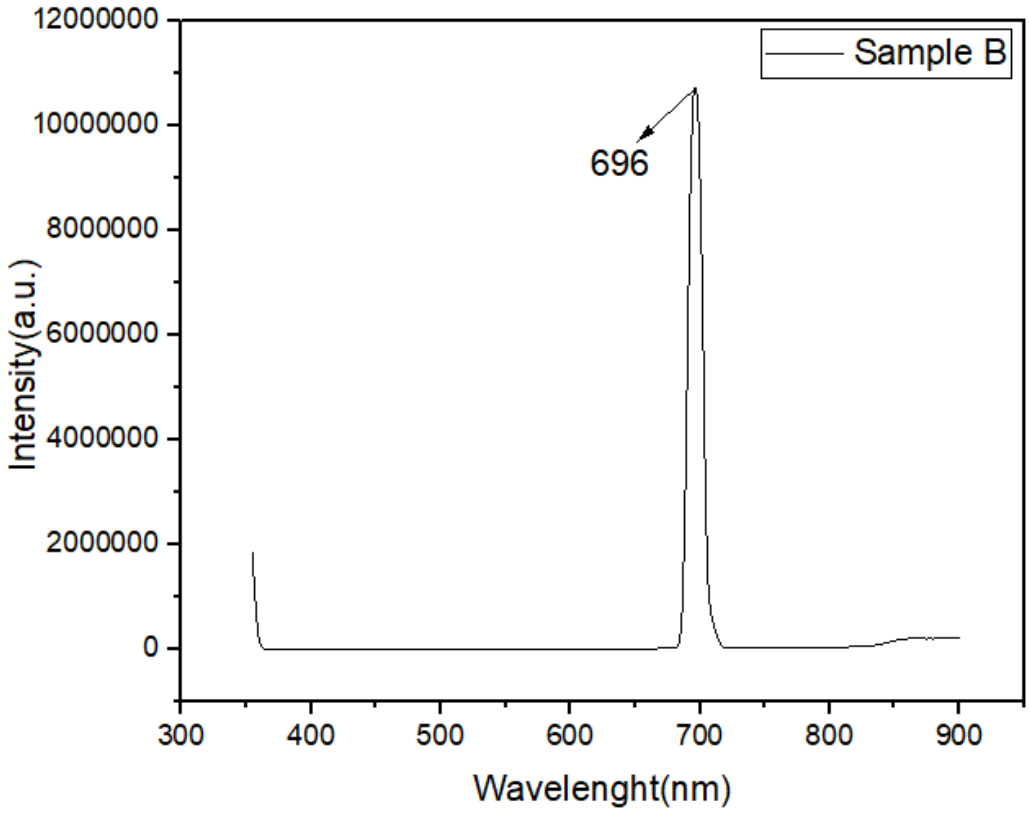

Figure 36: Emission spectra of Sample B

Photoluminescence is a process in which a molecule absorbs a photon in the visible region, exciting one of its electrons to a higher electronic excited state, and then radiates a photon as the electron returns to a lower energy state [56].
A light of different wavelength within is passed through monochromator, the function of monochromator is to pass only one specific wavelength after passing through it. After passing through monochromator, we get a monochromatic light with single wavelength. Now this monochromatic light falls on the sample surface which this monochromatic light and after certain time it re-emits in form of spectra which is called as emission spectra. The emission spectra are further passed through monochromator to get monochromatic emission light which is then passed through a detector which records the intensity as a function of emission wavelength and gives a plot [57].

The Photoluminescence excitation spectra of BBiT powder heat-treated at 500ºC for 5 hours has been measured in the wavelength range 350–950 nm. Excitation wavelength was 350 nm. As shown in Fig 36, the maximum PL intensity was shown at the wavelength of 696 nm with the corresponding excitation wavelength of 350 nm.

Following formula can be used to calculate energy gap-

$$E = hc/\lambda$$

Where E=energy gap, c=speed of light, h=Planck constant, λ=Wavelenght

Energy Gap corresponding to Excitation wavelength 350 nm = 3.54 eV
Energy Gap corresponding to Emission wavelength 696 nm = 1.78 eV

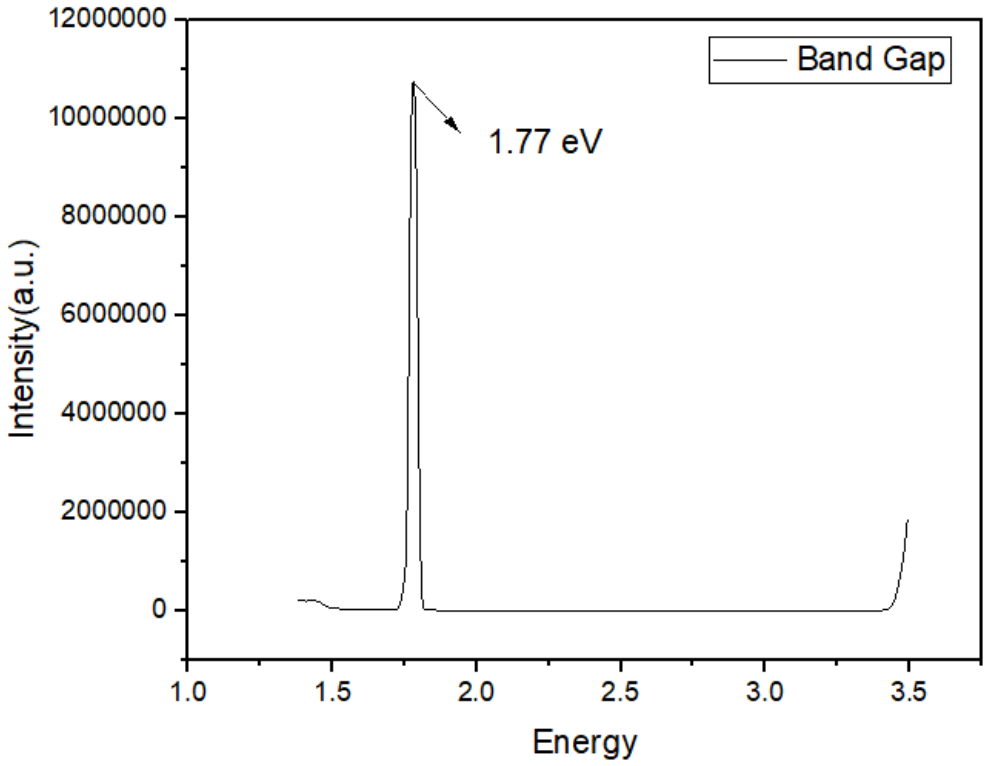

Figure 37: Band Gap of Sample B

Fig 38 shows band gap of Sample B during the emission of Sample B after excited by the wavelength 350 nm. A band gap of 1.77 eV is shown in the fig 38 which is lesser than the band gap during absorbance indicating that higher wavelength must be emitted after absorbance (696 nm > 350 nm).

We have converted emission onset wavelength into electron volt which give the difference between ground state and lowest excited state, which is known as band gap. Emission spectra are usually solvent dependent and are shifted with change in solvent polarity due to solvent relaxation so the absorption spectra are preferred for band gap calculations [58].

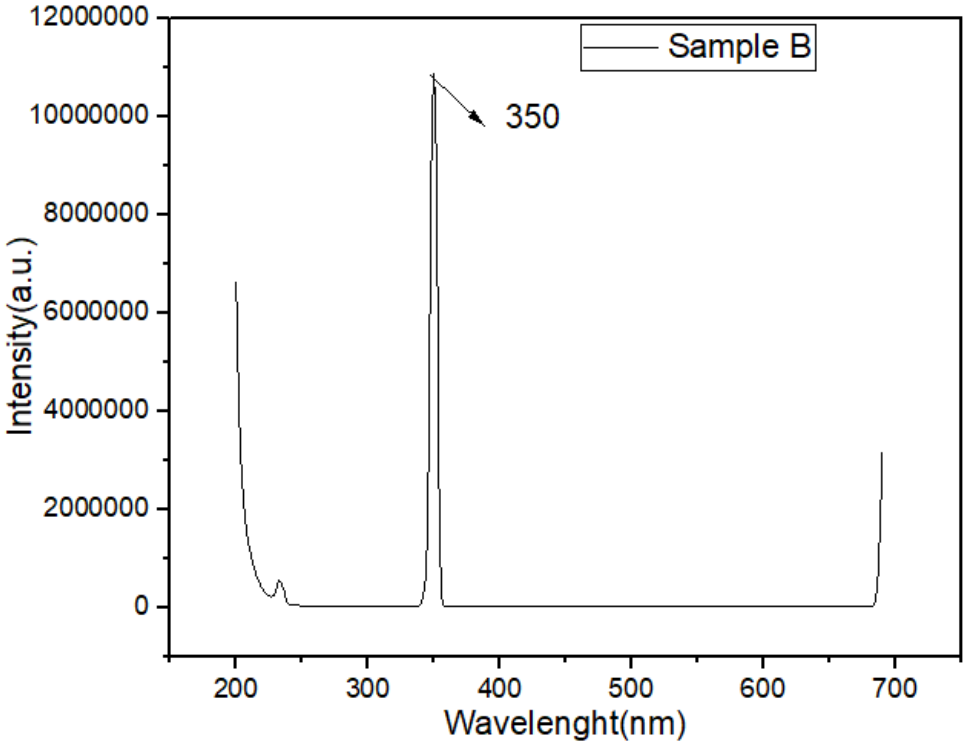

Figure 38: Absorbance spectra of Sample B

The Fig 38 shows the absorbance spectra of Sample B for the Emission wavelength 696 nm. The excitation wavelength come out to be 350 nm which is in accordance with the Emission spectra.

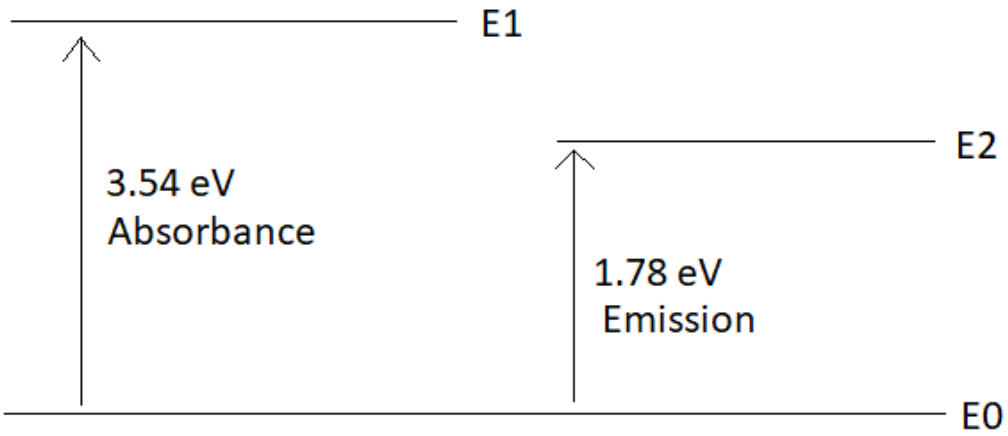

Figure 39: Energy Level before and after absorbance

Fig 40 shows the energy level during absorbance and emission of monochromatic light.

E1-E0 = Energy level difference between ground state and absorbance state = 3.54 eV
E2-E0 = Energy level difference between emission state and ground state = 1.78 eV
E1-E2= Shows nonradiative relaxation = 3.54-1.78= 1.76 eV

5.5 FESEM

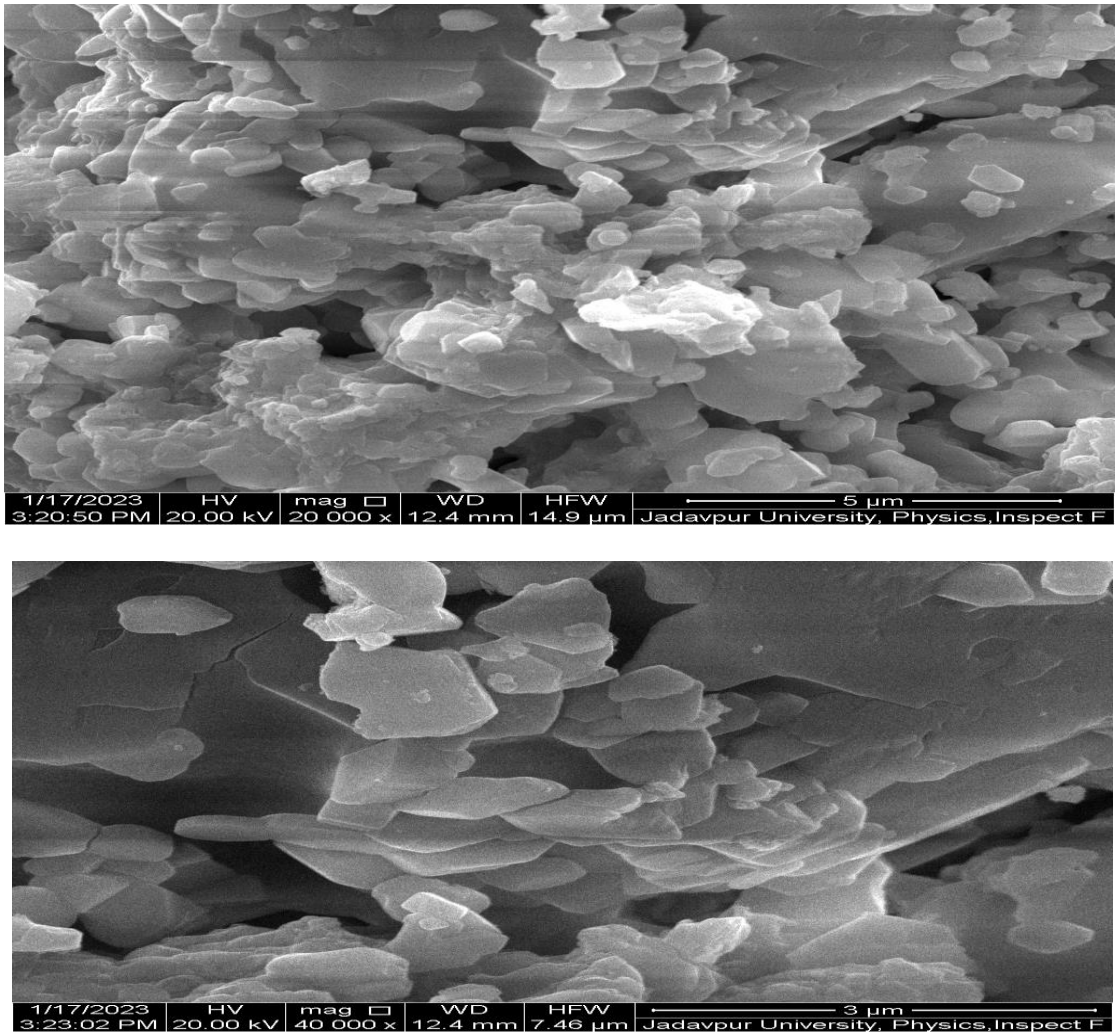

Figure 40: FESEM images of Sample B

FESEM morphology indicates dense agglomerates with negligible porosity. Particulates are rectangular
parallelopipeds polygon shape with some spherical in shape. Individual particulates are close to 100-300nm in
dimensions. Agglomerates are irregular shaped with slight flakes. Irregular fracture is noted in some portions with some elongated grains [59].

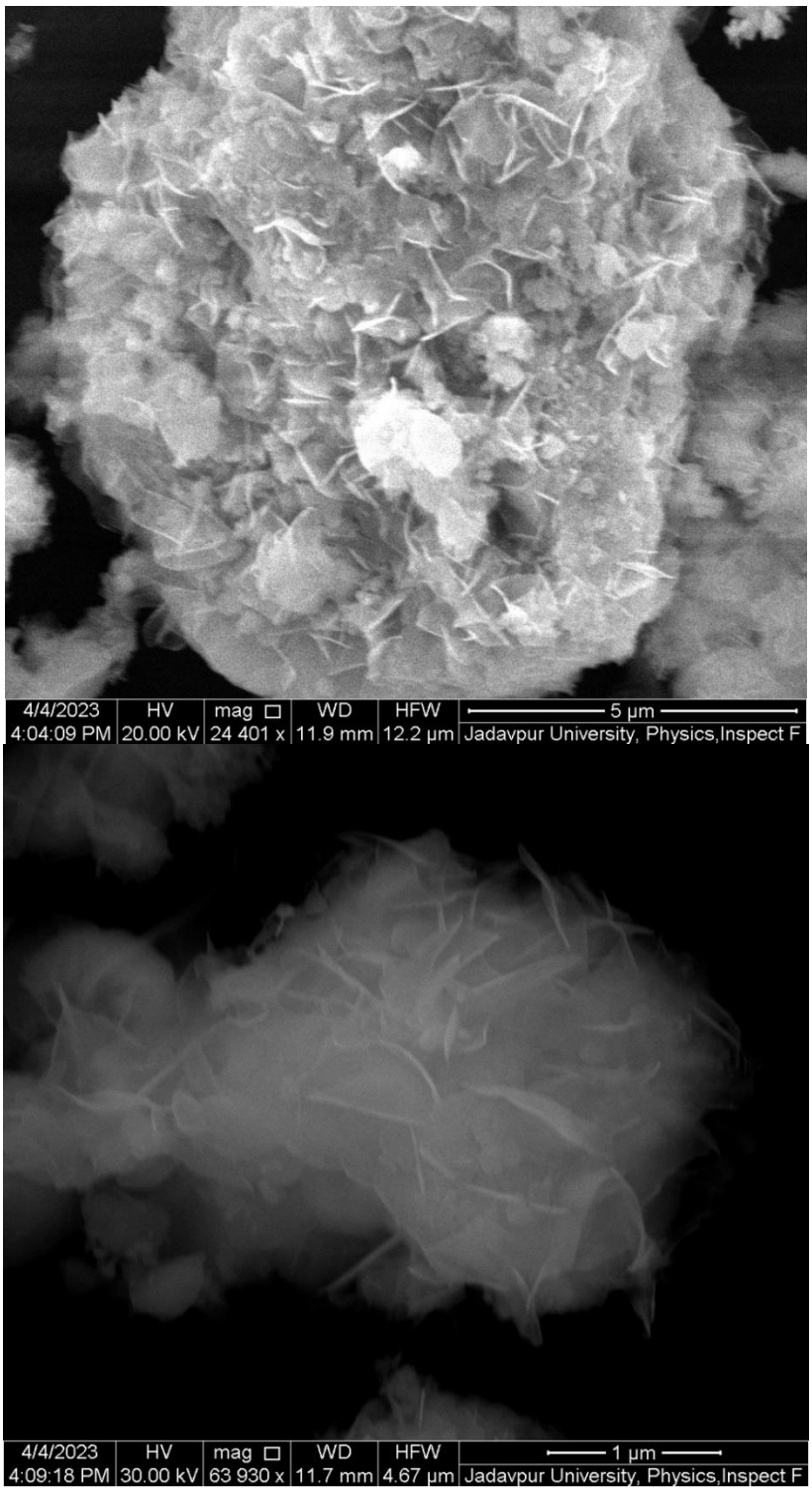

Figure 41: FESEM of doped sample D(x=0.05)

FESEM morphology of doped sample D has very high dense agglomerates with compared to undoped sample B. The morphology is noted to have agglomeration while the agglomerated chunks have irregular shape. Individual particulates are having spherical to irregular polygon shape with few interconnected pores. For a certain level of the amount of iron doping, the porosity decreases. One of the reasons may be due to fineness particles of Iron having radius about 125 nm, it fills the pore space of the undoped sample [60]. Particulates are some plates like shape with some spherical condensed agglomerates. Individual particulates are close to 50 nm in dimensions but

some particulates sizes are very small close to 7-10 nm in dimensions calculated using Scherrer formula. Average particulates size is about 25 nm. Agglomerates chunks are very irregularly shaped. Individual particulates are having spherical to irregular polygon shape. Irregular fracture is noted in some portions with some elongated grains.

CHAPTER 6
Conclusion and Future scope

Barium bismuth titanate was successfully synthesized using modified sol gel process. Heat treatment was carried for 6, 5, 4 hours at 400°C, 500°C and 550°C. Crystallite size was estimated to be about 40 nm, 42nm and 29 nm respectively from XRD curve using Scherrer equation. Iron doped BBiT was also synthesized at 3 different concentrations of iron (x=0.05, 0.075, 0.1). Crystallite sizes for doped BBiT were 23 nm, 17 nm and 16 nm respectively. Crystallite sizes decreases as the concentration of iron increases. DSC- TGA was carried to yield information on crystallization of ceramic phase development. FTIR analysis exhibits the required M-O co-ordinations of Si-O-Si bonds, Bi-O bonds and Ti-O bonds respectively. Morphology by SEM exhibits agglomeration tendency while individual particulates were noted to be rectangular parallelopiped polygon shape with some in spherical shape. BBiT powder has shown maximum emission spectra of 696 nm for the excitation wavelength of 350 nm and band gap of 1.78 eV.

The synthesized BBiT powder can be further characterized by TEM analysis to direct measurement of nanoparticle size, grain size, size distribution, and morphology. Microhardness can also be carried to determine hardness of BBiT pellets. Doped sample should have higher hardness than undoped sample. Also, hardness increases with increase in heat treatment time.

References

[1] Y. K. B. A. H. I. K. K. Brendan J. Kennedy, “Structural phase transitions in the layered bismuth oxide BaBi4Ti4O15,” *Solid State Communications*, pp. 653-658, 2003.

[2] W. P. Dan Xie, "Study on BaBi4Ti4O15 nanoscaled powders prepared by sol–gel method," *Materials Letters*, vol. 57, no. 19, p. 2970 – 2974, 2003.

[3] P. B. D. B. J. D. M. J. Tellier, "Structure versus relaxor properties in Aurivillius," *European Ceramic Society*, p. 3687–3690, 2007.

[4] P. B. M. M. a. D. M. J. Tellier, "A comparative study of the Aurivillius phase ferroelectrics CaBi4Ti4O15 and BaBi4Ti4O15," *Solid State Chemistry*, p. 1829–1837, 2004.

[5] X. M. C. Y. Z. R. Z. Hou, "Diffuse Ferroelectric Phase Transition and Relaxor Behaviors in," *The American Ceramic Society*, pp. 2839-2844, 2006.

[6] J. B. T. S. A. Chakrabarti, "Dielectric properties of BaBi4Ti4O15 ceramics produced by cost-effective," *Physica B*, p. 1498–1502, 2009.

[7] L. E. Cross, "Relaxorferroelectrics: An overview," *Ferroelectric*, vol. 151, pp. 305-320, 1994.

[8] T. K. A. H. Q. Z. B. K. Y. K. K. K. Ismunandar, "Structural studies of five layer Aurivillius oxides: A2Bi4Ti5O18 (A=Ca, Sr, Ba and Pb)," *Solid State Chemistry*, vol. 177, p. 4188–4196, 2004.

[9] A. J. R. M. Vaibhav Shrivastava, "Structural distortion and phase transition studies of Aurivillius type Sr1KxPbxBi2Nb2O9 ferroelectric ceramics," *Solid State Communications*, vol. 133, p. 125–129, 2005.

[10] S. N. V. R. A. Vadivel Murugan, "Preparation of nanocrystalline ferroelectric BaBi4Ti4O15 by Pechini method," *Materials Letters*, vol. 60, p. 1023–1025, 2006.

[11] J. S. Benjamin, "Mechanical Alloying," *Scientific American*, vol. 234, pp. 40-49, 1976.

[12] J. X. D. W. B. G. John Wang, "Mechanically Activating Nucleation and Growth of Complex Perovskites," *Solid State Chemistry*, vol. 154, no. 2, pp. 321-328, 2000.

[13] A. M. T. C. S. B. A. K. M. K. v. B. Troy B. Holland, "Field assisted sintering of nickel nanoparticles during in situ transmission electron microscopy," *Applied Physics Letters*, vol. 96, no. 24, 2010.

[14] Č. Jovalekić, M. Pavlović, P. Osmokrović and L. Atanasoska, "X-ray photoelectron spectroscopy study of Bi4Ti3O12 ferroelectric ceramics," *Appl. Phys. Lett.*, vol. 72, p. 1051–1053, 1998.

[15] B. J. R. N. P. N. S. B. Lazarević Z.Ž., "Study of barium bismuth titanate prepared by mechanochemical synthesis," *Science of Sintering*, vol. 41, no. 3, pp. 329-335, 2009.

[16] V. A. Isupov, "Crystal chemical aspects of the bismuth-containing layered compounds of the Am−1Bi2BmO3m+3 type," *Ferroelectrics*, vol. 189, pp. 211-227, 2011.

[17] J. D. RW Wolfe, vol. 6, pp. 1029-40, 1971.

[18] R. E. J. P. Z. P. C. Y. T. L. B. J. S. J. G. D. J. Taylor, "Electrical properties of SrBi2Ta2O9 thin films and their temperature dependence for ferroelectric nonvolatile memory applications," *Appl. Phys. Lett.* , vol. 68, p. 2300–2302, 1996.

[19] H. N. Y. H. Tadashi Takenaka, "Phase Transition Temperatures and Piezoelectric Properties of (Bi1/2Na1/2)TiO3-and (Bi1/2K1/2)TiO3-Based Bismuth Perovskite Lead-Free Ferroelectric Ceramics," *IEEE Transactions on Ultrasonics, Ferroelectrics, and Frequency Control*, vol. 56, no. 8, 2009.

[20] W. P. Z.-M. D. T.-l. R. Dan Xie, "Fabrication and Ferroelectric Properties of Ba-doped Strontium Bismuth Titanate Ceramics," *Key Engineering Materials*, Vols. 280-283, pp. 163-166, 2005.

[21] N. D. K. S. C. M.N. Kamalasanan, "Structural and microstructural evolution of barium titanate thin films deposited by the solgel process," *Applied Physics*, vol. 46, 1994.

[22] M. S. G.H. Yi, *Sol Gel Sci. and Tech*, vol. 6, p. 75, 1996.

[23] M. P. L. A. C Jovalekic, "X-ray photoelectron spectroscopy study of Bi 4 Ti 3 O 12 ferroelectric ceramics," *Applied Physics Letters*, vol. 72, 1998.

[24] C. P.-S. C. J. A. S. F. F. Z. L. J. V. Biljana D. Stojanovic, "Mechanically activating formation of layered structured bismuth titanate," *Materials Chemistry and Physics*, vol. 96, no. 2-3, pp. 471-476,

2006.

[25] J. B. N. Ž. R. N. P. B. D. S. Z. Ž. Lazarević, "Study of Barium Bismuth Titanate Prepared by Mechanochemical Synthesis," *Science of Sintering,* vol. 41, pp. 329-335, 2009.

[26] V. M. M. R. T. S. B. D. Bobić Jelena D., "Characterization and properties of barium bismuth titanate," *Processing and Application of Ceramics,* vol. 3, no. 1-2, pp. 9-12, 2009.

[27] K. B. R. V. Sunil Kumar, "Influence of lanthanum doping on the dielectric, ferroelectric and relaxor behaviour of barium bismuth titanate ceramics," *Applied Physics,* vol. 42, 2009.

[28] D. Viehland, S. J. Jang, L. E. Cross and M. Wuttig, "Freezing of the polarization fluctuations in lead magnesium niobate relaxors," *Applied Physics,* vol. 68, 1990.

[29] K. V. Sunil Kumar, "Dielectric relaxation in bismuth layer-structured BaBi4Ti4O15 ferroelectric ceramics," *Current Applied Physics,* vol. 11, no. 2, pp. 203-210, 2011.

[30] M. V. S. G. J. B. B. S. J.D. Bobić, "Dielectric and relaxor behavior of BaBi4Ti4O15 ceramics," *Journal of Alloys and Compounds,* vol. 499, no. 2, pp. 221-226, 2010.

[31] I. M. R. W. E. L. Donají Y. Suárez, "Relation between tolerance factor and Tc in Aurivillius compounds," *Journal of Materials Research,* vol. 16, no. 11, pp. 3139-3149, 2011.

[32] M. V. P. J. B. B. S. J.D. Bobic´, "Electrical properties of niobium doped barium bismuth-titanate ceramics," *Materials Research Bulletin,* vol. 47, p. 1874–1880, 2012.

[33] J. E. Shelby, Introduction to Glass Science and Technology, USA: Royal Society of Chemistry, 2005.

[34] A. T. B. K. Atiar Rahaman Molla, "Fabrication and properties of Nd3þ-doped ferroelectric barium bismuth titanate glass-ceramic nanocomposites," *Journal of Alloys and Compounds,* vol. 680, pp. 237-246, 2016.

[35] "Tempsens," [Online]. Available: https://tempsens.com/blog/tubular-furnace.

[36] Y. T. F. S. D. K. U. Satoshi Tanaka, "Fabrication of crystal-oriented barium-bismuth titanate ceramics in high magnetic field and subsequent reaction sintering," *SCIENCE AND TECHNOLOGY OF ADVANCED MATERIALS,* vol. 10, 2009.

[37] D. Banerjee, "X-Ray Diffraction," [Online]. Available: https://www.iitk.ac.in/che/pdf/resources/XRD-reading-material.pdf.

[38] Madhusha, "Difference Between TGA DTA and DSC," 5 October 2017. [Online]. Available: https://pediaa.com/difference-between-tga-dta-and-dsc/.

[39] A. Balekundri, "Thermo gravimetric analysis(tga)," Slideshare, 2 June 2019. [Online]. Available: https://www.slideshare.net/AmrutaBalekundri/thermo-gravimetric-analysistga.

[40] ScienceDirect, [Online]. Available: https://www.sciencedirect.com/topics/engineering/field-emission-scanning-electron-microscope.

[41] A. Nanakoudis, "EDX Analysis with SEM: How Does it Work?," ThermoFisher Scientific, 28 11 2019. [Online]. Available: https://www.thermofisher.com/blog/materials/edx-analysis-with-sem-how-does-it-work/#:~:text=The%20way%20EDX%20analysis%20works,shell%20to%20fill%20the%20vacancy..

[42] "FTIR: Fourier-Transform Infrared Spectroscopy Principles and Applications," FindLight, 27 March 2019. [Online]. Available: https://www.findlight.net/blog/ftir-principles-applications/.

[43] "Innovative and versatile FTIR spectroscopy software and libraries," ThermoFisher Scientific, [Online]. Available: https://www.thermofisher.com/in/en/home/industrial/spectroscopy-elemental-isotope-analysis/molecular-spectroscopy/fourier-transform-infrared-spectroscopy/software.html.

[44] "Principles of infrared spectroscopy (4) Advantages of FTIR spectroscopy," Jasco, [Online]. Available: https://www.jasco-global.com/principle/principles-of-infrared-spectroscopy-4-advantages-of-ftir-spectroscopy/#:~:text=1.,%2Fprism%20(Fellgett's%20advantage)..

[45] D. Heiman, "Photoluminescence Spectroscopy," Physics U600, Adv Lab I – Physics of Waves and Optics – Summer 2004, Northeastern University, 2004.

[46] J. REICHMAN, HANDBOOK of OPTICAL FILTERS for FLUORESCENCE MICROSCOPY, CHROMA TECHNOLOGY CORP, 2017.

[47] C. R. Ronda, Luminescence: From Theory to Applications, WILEY-VCH, 2007.

[48] A. R. B. Ruquan Ye, "PHOTOLUMINESCENCE SPECTROSCOPY AND ITS APPLICATIONS," OPENSTAX-CNX.

[49] *XRD interpretations for doping,* Pakistan: Youtube, 2022.

[50] M. P. V. N. K. U. A. B. N. MANJULA, "Effect of doping concentration on the structural, morphological, optical and electrical properties of Mn-doped CdO thin films," *Materials Science-Poland,* vol. 33, no. 4, pp. 774-781, 2015.

[51] "Interplanar Spacing of Tetragonal Lattice Calculator," Calistry, 2015. [Online]. Available: http://calistry.org/calculate/spacingTetragonalLattice.

[52] NanoWorld, "How to calculate lattice constant (a,b,c) values of a unit cell from XRD data-12," Youtube, United Kingdom, 2019.

[53] M. Farahmandjou, "Synthesis and characterization of alpha-Fe2O3 nanoparticles by aimple co-precipation method," *Physical Chemistry Research,* vol. 3, 2015.

[54] H. Azzam, "What are the values of wavenumber for silica in FT-IR spectrum?," Researchgate, University of Jordan, 2019.

[55] N. V. P. M. S. G. P. T Sravan Rao, "Synthesis and Characterization of Bismuth Borate-Barium Titanate Glass Ceramics," *Indian Journal of Science and Technology,* vol. 15, no. 17, pp. 839-849, 2022.

[56] J. Mitrić, "Photoluminescence Spectroscopy," sciencedirect, 2022.

[57] Spatium, "Photoluminescence Spectrometer," Youtube, India, 2019.

[58] G. Singh, "How to determine the band gap of a materialfrom PL spectra.," ResearchGate, Florida, 2016.

[59] M. S. S. B. SOUMYA MUKHERJEE, "Phase Development of Barium Bismuth Titanate by Modified Solid State Route," *Material Science Research India,* vol. 17, no. 2, pp. 129-135, 2020.

[60] R. M. J. T. Moussa Anan Largeau, "Effect of Iron Powder on Strenght, Workability, and Porosity of the binary blended concrete," *Open Journal of Civil Engineering,* vol. 8, no. 4, 2018.

Appendix
1. Calculation

1.1 Undoped Barium Bismuth Titanate

Molar mass of $Bi(NO_3)_3 \cdot 5H_2O$ is 485.07 gm/mol
Molar mas of Bismuth is 208.98 gm/mol
Mass ratio of Bismuth in Bismuth nitrate= (208.98/485.07)*100 =43.0824 %

Molar mass of $Ti(OC_4H_9)_4$ is 340.327 gm/mol
Molar mas of Titanium is 47.867 gm/mol
Mass ratio of Titanium in Tetrabutyl Titanate=(47.867/340.327)*100 =14.065 %

Molar mass of $Ba(CH_3COO)_2$ is 255.416 gm/mol
Molar mas of Barium is 137.328 gm/mol
Mass ratio of Barium in Barium Acetate= (137.328/255.416)*100 =53.7664 %

That means if we take 20 gm of $Bi(NO_3)_3 \cdot 5H_2O$ then it will have 8.6164 gm of Bismuth in it.
Mole of Bismuth=8.6164/208.98 =0.0412
Now since mole ratio of Ba, Bi and Ti is 1:4:4 therefore,

Mole of Barium=0.0412/4=0.0103
Mole of Titanium=0.0412/1=0.0412

Mass of Barium=0.0103*137.328 =1.414 gm
Mass of Titanium=0.0412*47.867=1.9721 gm

Amount of Barium Acetate required for 1.414 gm of Barium =(100/53.7664)*1.414 =2.6298 gm

Amount of Tetrabutyl Titanate required for 1.9721 gm of Titanium=(100/14.065)*1.9721 =14.0213 gm

1.2 Iron doped Barium Bismuth Titanate

Iron will take place of Bismuth in Iron doped BBiT as follows $BaBi_{4-x}Fe_xTi_4O_{15}$ where x=0.05, 0.075 and 0.1

When x=0.05

We know 10 gm of $Bi(NO_3)_3 \cdot 5H_2O$ has 4.3082 gm of Bismuth or 0.0206 mole of Bismuth in it.
Now substituting x=0.05 we get $BaBi_{3.95}Fe_{0.05}Ti_4O_{15}$ which means ratio of

Ba:Bi:Fe:Ti=1:3.95:0.05:4

Fe doped with the help of compound Ferric Nitrate Nonahydrate $Fe(NO_3)_3.9H_2O$ having molecular weight 403.992 gm/mol.

Therefore, Mass ratio of Fe in $Fe(NO_3)_3.9H_2O$= (55.845/403.992)*100 = 13.82329 %

Mole of Barium= (0.0206/3.95)*1= 0.0052151899
Mass of Barium= 0.0052151899*137.328= 0.716191 gm
Amount of Barium Acetate required for 0.716191 gm of Barium= (100/53.7664)*0.716191 = 1.332 gm

Mole of Titanium= (0.0206/3.95)*4=0.0208607596
Mass of Titanium= 0.0208607596*47.867= 0.9985419 gm
Amount of Tetrabutyl Titanate required for 0.9985419 gm of Titanium= (100/14.065)*0.9985419 = 7.09948 gm

Mole of Fe= (0.0206/3.95)*0.05= 0.0002607595
Mass of Fe= 0.0002607595*55.845= 0.014562 gm
Amount of $Fe(NO_3)_3.9H_2O$ required for 0.014562 gm of Fe= (100/13.82329)*0.014562 = 0.1053439 gm

When x=0.075

x=0.075 gives $BaBi_{3.925}Fe_{0.075}Ti_4O_{15}$ which means ratio of Ba:Bi:Fe:Ti=1:3.925:0.075:4

Mole of Barium= (0.0206/3.925)*1= 0.0052484076
Mass of Barium= 0.0052484076*137.328= 0.7205013953 gm
Amount of Barium Acetate required for 0.7205013953 gm of Barium= (100/53.7664)*0.7205013953 = 1.34 gm

Mole of Titanium= (0.0206/3.925)*4=0.0209936304
Mass of Titanium= 0.0209936304*47.867= 1.0049021064 gm
Amount of Tetrabutyl Titanate required for 1.0049021064 gm of Titanium= (100/14.065)*1.0049021064 = 7.1447003655 gm

Mole of Fe= (0.0206/3.925)*0.075= 0.0003936306
Mass of Fe= 0.0003936306*55.845= 0.0219823009 gm
Amount of $Fe(NO_3)_3.9H_2O$ required for 0.0219823009 gm of Fe= (100/13.82329)*0.0219823009 = 0.159 gm

When x=0.1

x=0.1 gives $BaBi_{3.9}Fe_{0.1}Ti_4O_{15}$ which means ratio of Ba:Bi:Fe:Ti=1:3.9:0.1:4

Mole of Barium= (0.0206/3.9)*1= 0.005282051
Mass of Barium= 0.005282051*137.328= 0.72537353 gm
Amount of Barium Acetate required for 0.72537353 gm of Barium= (100/53.7664)*0.72537353 = 1.3491205 gm

Mole of Titanium= (0.0206/3.9)*4=0.0211282051

Mass of Titanium= 0.0211282051*47.867= 1.01134379 gm
Amount of Tetrabutyl Titanate required for 1.01134379 gm of Titanium= (100/14.065)*1.01134379 = 7.1904998102 gm

Mole of Fe= (0.0206/3.9)*0.1= 0.00052820512
Mass of Fe= 0.00052820512*55.845= 0.0294976153 gm
Amount of $Fe(NO_3)_3.9H_2O$ required for 0.0294976153 gm of Fe=(100/13.82329)*0.0294976153

= 0.2133906892 gm

2. Lattice Constant Calculation

Equation of interplanar spacing for a Tetragonal unit cell- $\frac{1}{d^2} = \frac{h^2+k^2}{a^2} + \frac{l^2}{c^2}$------1
d can be calculated by the Bragg's law given by- $n\lambda = 2dsin\theta$---------2
In sample B, miller indices corresponding to peaks of 2ϴ angles 21.69283and 30.95601 are (0 0 10) and (1 1 0).

Take n=1

$$1 * 1.54006 = 2 * d * \sin\left(rad(\frac{21.69283}{2})\right)$$

$$d = \frac{1.5406}{2*\sin\left(rad(\frac{21.69283}{2})\right)}$$

$$d = 4.093486 \text{ Å}----------3$$

Now take miller indices (0 0 10) corresponding to angle 21.69283 and d=4.093486 and put it in equation 1,

We get $$\frac{1}{d^2} = \frac{h^2+k^2}{a^2} + \frac{l^2}{c^2}$$

$$\frac{1}{(4.093486)^2} = \frac{0^2+0^2}{a^2} + \frac{10^2}{c^2}$$

$$c = 40.93486 \text{ Å}$$

Now again take miller (1 1 0) corresponding to angle 30.95601,

$$1 * 1.5406 = 2 * d * \sin\left(rad\left(\frac{30.95601}{2}\right)\right)$$

$$d = \frac{1.5406}{2*\sin\left(rad\left(\frac{30.95601}{2}\right)\right)}$$

$$d = 1.4142135623 \text{ Å}$$

Putting d=1.4142135623 Å and (1 1 0) in equation 1, we get

$$\frac{1}{d^2} = \frac{h^2+k^2}{a^2} + \frac{l^2}{c^2}$$

$$\frac{1}{1.4142135623^2} = \frac{1^2+1^2}{a^2} + \frac{0^2}{c^2}$$

$$a = 4.0832044$$